Arabian Journal of Geosciences (2020) 13: 732
https://doi.org/10.1007/s12517-020-05697-w

ORIGINAL PAPER

A semi-quantitative landslide risk assessment of central Kahramanmaraş City in the Eastern Mediterranean region of Turkey

Çiğdem Tetik Biçer[1] · Murat Ercanoglu[2]

Received: 17 February 2020 / Accepted: 9 July 2020 / Published online: 25 July 2020

Abstract
Landslides are one of the most destructive natural hazards in Turkey. In addition to loss of lives, there were many negative impacts of landslides on properties and the environment. To minimize the losses and damages related to landslides, a series of labour-intensive studies starting from landslide inventory to landslide risk mapping is required. Thus, this study aims to assess the landslide risk by a semi-quantitative approach in a landslide-prone area located in the Eastern Mediterranean region of Turkey. This region has been suffering from landslides with its high population and industrial characteristics. A total of 215 deep-seated rotational earth slides were mapped during field studies. Then, landslide-susceptibility mapping was performed by frequency ratio and logistic regression methods. For the hazard stage, the susceptibility map and the triggering indicator maps were used to produce a Landslide Hazard Index (LHI) map. As for the vulnerability analysis, a relative evaluation was performed by considering land use, infrastructure and population density data. All maps were combined at the final stage to produce a Landslide Risk Index (LRI) map of the study area. It was revealed that areal coverages of the produced LRI map were 21.4% very low (VL), 10.8% as low (L), 37.4% as medium (M), 24.8% as high (H) and 5.6% as very high (VH) LRI, respectively. The so-produced LRI map would be beneficial for further and detailed risk analyses to be performed in the future since it highlights the landslide risk hotspots in a regional scale.

Keywords GIS · Kahramanmaraş · Landslide · Landslide risk · Semi-quantitative assessment

Introduction

As declared in the 4th World Landslide Forum, the 2017 Ljubljana Declaration on landslide risk reduction and the Kyoto 2020 Commitment will shape the future works related to landslide studies throughout the world in the next years. These efforts particularly aim to strengthen networking with governments for landslide risk reduction (Sassa 2017), similar to the previous scientific attempts such as Aleotti and Chowdhury (1999), Fell et al. (2008a, 2008b) and Corominas et al. (2014). All these studies are excellent guides for any landslide-related study considering almost every aspect of the idealized procedures related to these works. However, landslides and their undesirable effects have still been a problematic issue throughout the world despite such important efforts. This situation could be explained by the fact that insufficient attention is still paid by the decision makers, politicians and local administrations as well as the people. It could be concluded that one of the most important aspects of the 4th Landslide Forum is emphasizing the importance of responsibilities of the governments and decision makers on the landslide mitigation efforts, including people living in the hazardous regions.

Landslide maps of any type are required for a safer urbanization and environment, land use and regional development plans. Of these, landslide-susceptibility and hazard studies were more performed by the researchers in the landslide literature. However, landslide risk was not a frequent topic in the landslide literature (Bednarik et al. 2012). Nonetheless, landslide inventory and database preparation stage, a key to

Responsible Editor: Zeynal Abiddin Erguler

✉ Murat Ercanoglu
murate@hacettepe.edu.tr

Çiğdem Tetik Biçer
cigdem.tetik@afad.gov.tr

[1] Turkey Ministry of Interior, Disaster and Emergency Management Authority, Üniversiteler Mahallesi Dumlupınar Bulvarı, No: 159, Çankaya, 06800 Ankara, Turkey

[2] Geological Engineering Department, Hacettepe University, Beytepe, 06800 Ankara, Turkey

whatsoever landslide study, is by far the most significant step. As Ye et al. (2019) stated, detecting and monitoring landslides are hot topics in the remote sensing community, particularly with the development of remote sensing (RS) technologies and the significant progress of computer vision. In this context, RS techniques such as aerial photography, high- or medium-resolution optical satellite images, interferometric synthetic aperture radar (InSAR) and light detection and ranging (LiDAR) were widely used in landslide studies (Alkevli and Ercanoglu 2011; Pirasteh and Li 2017a; Pirasteh et al. 2020). Based on the perpetual developments of computer, geographical information system (GIS) and RS technologies at the end of the 1980s and 1990s, the scientific landslide literature has witnessed splendid progressions. On the one hand, more attention has been paid by scientists on landslide-related studies; on the other, data availability and quality, funding provided by local/governmental agencies and technological aspects have always increased during this period worldwide. Particularly, landslide-susceptibility mapping studies have been more preferred by the scientists using different quantitative and qualitative methods when compared with the landslide hazard and risk studies. The main reason could be related to the difficulties in producing a landslide hazard or risk map that could be considered as a more challenging task and needs more detailed data. In addition, incompleteness of the landslide inventory maps and absence of reliable damage data related to landslides could be considered as the two most important reasons in order to reach hazard and risk. Despite all, landslide hazard and risk could be evaluated by different approaches even in national and global scales in some studies such as Guzzetti et al. (2000), Evans and Roberts (2006), Nadim et al. (2006), Yoshimatsu and Abe (2006), Abella and Van Westen (2007), Van Den Eeckhaut and Herva´s (2012), Jaedicke et al. (2014) and Di Martire et al. (2017).

Although the term risk corresponds to various meanings in different disciplines, one of the most commonly used definitions of risk is the expected number of lives lost, persons injured, damage to property and disruption of economic activity due to a particular damaging phenomenon for a given area and reference period (Varnes and IAEG 1984). This definition is also known as the total risk (R_T), which is often difficult to calculate and is almost impossible particularly for medium- and small-scale studies. For the medium- and small-scale studies, the researchers preferred to use the term specific risk (R_S) (e.g. Abella and Van Westen 2007; Akgun et al. 2012; Bianchini et al. 2017). R_S is simply expressed by the product of hazard (H) and vulnerability (V) (Varnes and IAEG 1984). The term V means degree of loss to a given element, or set of elements, at risk resulting from the occurrence of a natural phenomenon of a given magnitude (Varnes and IAEG 1984). In this regard, we approached the specific risk term in this study by considering the available data and the scale. Details regarding the specific risk components (i.e. hazard, which also includes the susceptibility stage, and vulnerability) were given in the related sections of the study.

In this study, given the concepts above, a regional semi-quantitative landslide risk assessment was performed in Kahramanmaraş City centre and its vicinity, located in the Eastern Mediterranean region of Turkey. Since the landslides are one of the most problematic natural hazards in the city, it is aimed to highlight the landslide risk hotspots in a regional scale for the study area. To assess the landslide risk of the selected area, a semi-quantitative landslide risk index (LRI) was approached because of the fact that there were limited numerical data such as complete landslide inventory, occurrence dates of the landslides, quantitative damage information, etc. A semi-quantitative risk assessment could be considered as an intermediate stage between qualitative (heuristic) and quantitative (probabilistic) risk evaluations by ranking the risk of concern. In order to calculate the LRI in the study area, data provided by AFAD (Disaster and Emergency Management Presidency of Turkey) were used and updated during the field studies as much as possible. Then, landslide susceptibility, hazard and vulnerability assessments were performed. Finally, a semi-quantitative landslide risk assessment was conducted by producing an LRI map of the study area. All stages of the study were presented in detail in the next sections.

Study area

Kahramanmaraş City is located in the eastern part of the Mediterranean region of Turkey (Fig. 1), and has an extent of 14,525 km^2, comprising of 11 different provinces. The population of Kahramanmaraş is 1,075,706, and the northern part of the city mostly contains plain areas. In general, the city presents mountainous and semi-mountainous morphological features, and the Mediterranean climate is dominant in the region. The eastern and the southern parts have a rugged topography. The summers are hot and arid; the winters are warm and rainy. The months December and January are the rainiest ones with an average rainfall of around 120 mm. The highest temperature is observed in July and August (MGM 2019) (Table 1). The city is in a very important position in terms of industrial purposes, and there are two official and two privately organized industrial zones. For the textile industry, Turkey's largest organized industrial zone will be established in the city. The city has a feature that can be regarded as a centre for transportation and railway network in the Eastern Mediterranean region, connecting the Eastern and Southeastern Anatolia regions of Turkey.

Kahramanmaraş City has suitable geological, geomorphological and climatic characteristics in terms of natural disaster occurrences such as earthquakes, landslides, floods,

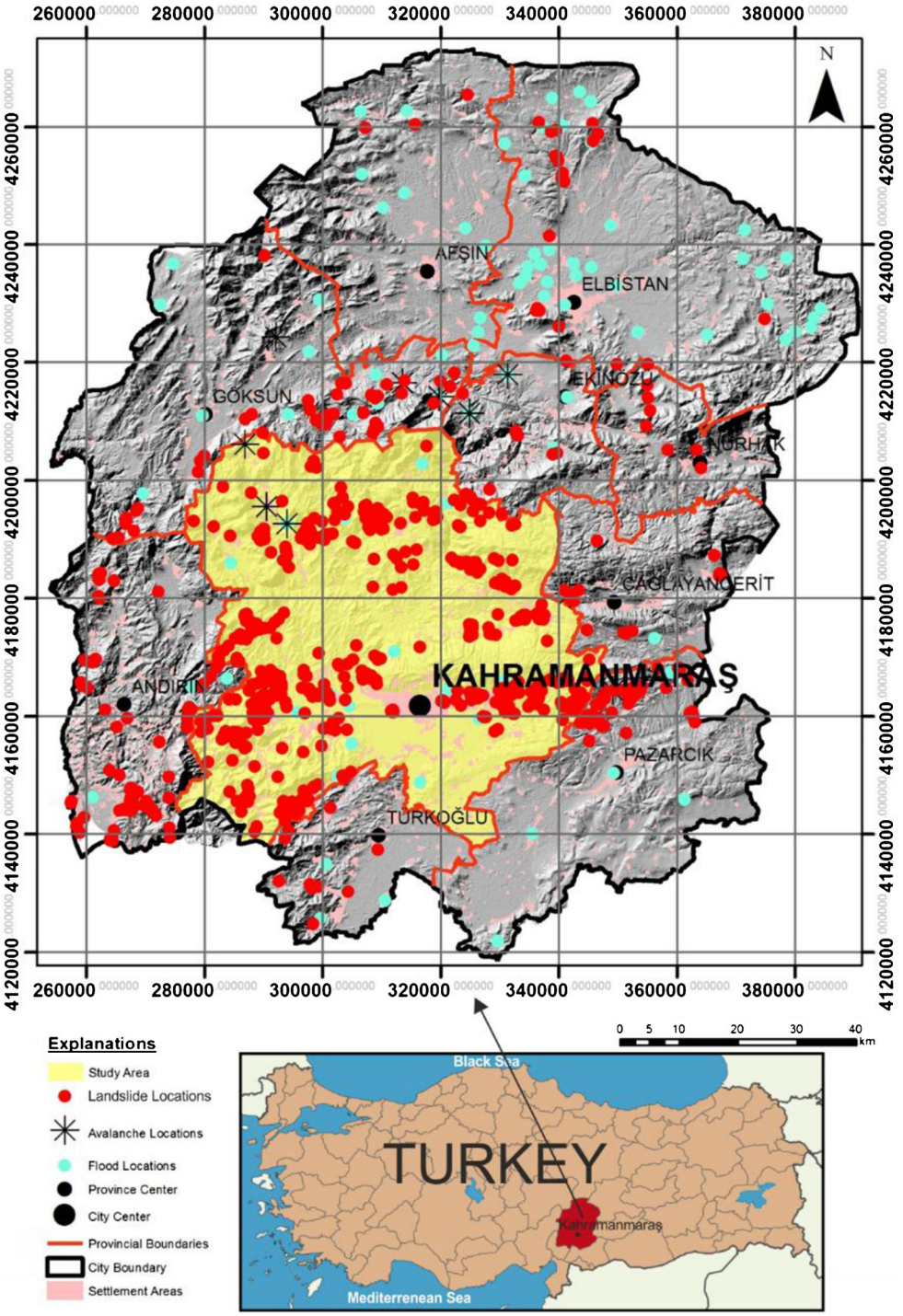

Fig. 1 Location map of the study area

Table 1 Monthly long-term meteorological characteristics of the region

	January	February	March	April	May	June	July	August	September	October	November	December
Average temperature (°C)	3.7	5.3	9.0	14.1	19.0	23.8	27.3	27.2	23.7	17.5	11.1	6.0
Maximum temperature (°C)	7.8	9.7	14.2	20.0	25.7	31.0	34.7	34.6	31.6	24.6	16.8	10.2
Minimum temperature (°C)	− 9.0	− 9.6	− 7.6	− 1.8	5.0	10.3	15.6	15.7	8.6	0.0	− 5.6	− 7.6
Average precipitation (mm)	120.1	102.3	91.8	68.7	39.0	10.1	3.1	4.2	8.3	45.0	70.5	121.2

avalanches, etc. For this reason, it is necessary to take into consideration the properties and the mechanisms of the natural disasters, particularly for the landslides that are the most commonly encountered disaster type in the city (see Fig. 1). However, if the spatial distribution of the landslides is considered, it is evident that the central part of the city contains more landslide locations as well as a bigger population and higher urbanization. For this reason, the central part of the city (see Fig. 1) was selected as the study area covering 3516 km^2 in order to assess the landslide risk.

With respect to the geological features, it can be concluded that Kahramanmaraş is located in a region where the geological and tectonic characteristics are complicated. In order to simplify the geological features, at this stage, they were grouped by their system/period and are shown in Fig. 2. Detailed lithological names and ages were also presented below this figure. There are 11 different lithological groups and 48 units ranging between the Precambrian to the Quaternary period (see Fig. 2). At the basement, Precambrian amphibolite, schists and gneisses are located. These units are overlaid by marble, gneiss, schists and dolomites of the Ordovician period. Silurian shale, sandstone alternations are overlaid by massive limestones of Devonian, quartzite and siltstone. Permian, Triassic and Jurassic units are mostly represented by limestone, dolomite, marble and calc-schist. In general, Cretaceous units are in flysch facies comprising conglomerate, sandstone, mudstone and marl alternations. The Paleogene period is mostly represented by limestone, sandstone and marl in addition to volcanic rocks, which were overlaid by Neogene units of conglomerate, sandstone, gypsum, tuff and marl. Neogene units were the most abundant lithological units in the study area. Quaternary units include alluvium and slope debris, mostly located in close vicinity to the city centre and along the rivers and steep slopes. The study area is very close to the Eastern Anatolian Fault Zone (EAFZ) at which many destructive earthquakes occurred before, and a few segments of the EAFZ pass through the SE part of the study area (see Fig. 2). In addition, thrusts developed mostly in the Eocene and Miocene and strike slip faults are commonly traced in the study area (Sümengen 2013).

The city centre is mostly covered by alluvial deposits and represents plain features with gentle slopes, while the other parts show generally moderate to high steep topographical features. Topographical elevation ranges between 203 and 3024 m (asl), and the eastern and northeastern parts of the study area have elevation values greater than 2000 m. Slope degrees range between 0 and 69°, and particularly, the SE and NE parts of the study area contain steep slopes greater than 45°, covered by massive and strong lithological units.

Landslides in the region were mapped and updated during the field studies. A total of 215 deep-seated rotational earth slides (Fig. 3a) were mapped during the field studies, and their areal extents ranged between 0.002 and 5.2 km^2 (Fig. 3b). It should be noted that the *x* axis of the landslide sizes in Fig. 3b represents the logarithm of the landslide sizes. It is very well-known that a detailed and reliable landslide inventory and database are essential for any landslide work. However, as in the case of this study, complete landslide inventory maps are lacking in many countries. Based on the archives and database of AFAD, it was not possible to obtain the exact dates of the all landslides, which was very important for the landslide hazard assessment stage for triggering factor analysis. Unfortunately, only the dates of 29 of the total landslides were exactly known (day/month/year) in the AFAD landslide archives and database (Fig. 3c). It was revealed that March and January were the two months that most of the landslides occurred. In addition, the occurrence years of the 71 landslides were only known in this database when compared with the Kahramanmaraş Meteorological Station (KMS) data (Fig. 3d). Although there are 11 rainfall stations in the city, they have many data deficiencies. There is only one rainfall station located in the city centre (i.e. KMS), including full daily rainfall data starting from 1959 to 2015 with a mean annual precipitation (MAP) of 718.5 mm (see Fig. 3d).

Even if the exact dates of all landslides were not known, it could be initially concluded that there was a good harmony between the number of landslides and rainfall amount, which could be considered as a key indicator to the hazard assessment. When Fig. 3d is examined, it could be concluded that there was a general agreement with the number of landslides and precipitation, particularly in 1976, 1987 and 2009, respectively. Unfortunately, the long-term data of KMS itself was not sufficient enough to model the landslide hazard throughout the study area. For example, some landslides, particularly located in the NW part of the study area, are highly far from the location of KMS (approximately 50 to 60 km). Thus, under these circumstances, it was not possible to assess the landslide hazard in the region based on the definition given by Guzzetti et al. (1999). The details related to the triggering factors can be found in the hazard section.

Methodology

Landslide susceptibility

In order to assess the landslide risk in a region, the second important stage following the landslide inventory studies is to evaluate the landslide susceptibility. Landslide susceptibility evaluations need to be able to respond to questions (e.g., where, under which conditions? etc.) that landslides are likely to occur in the future. The quality and the accuracy of these maps are also related to the purpose, scale, data and financial conditions of the study. In this context, the susceptibility phase after the inventory studies is very important for both hazard and risk stages. Landslide susceptibility assessment

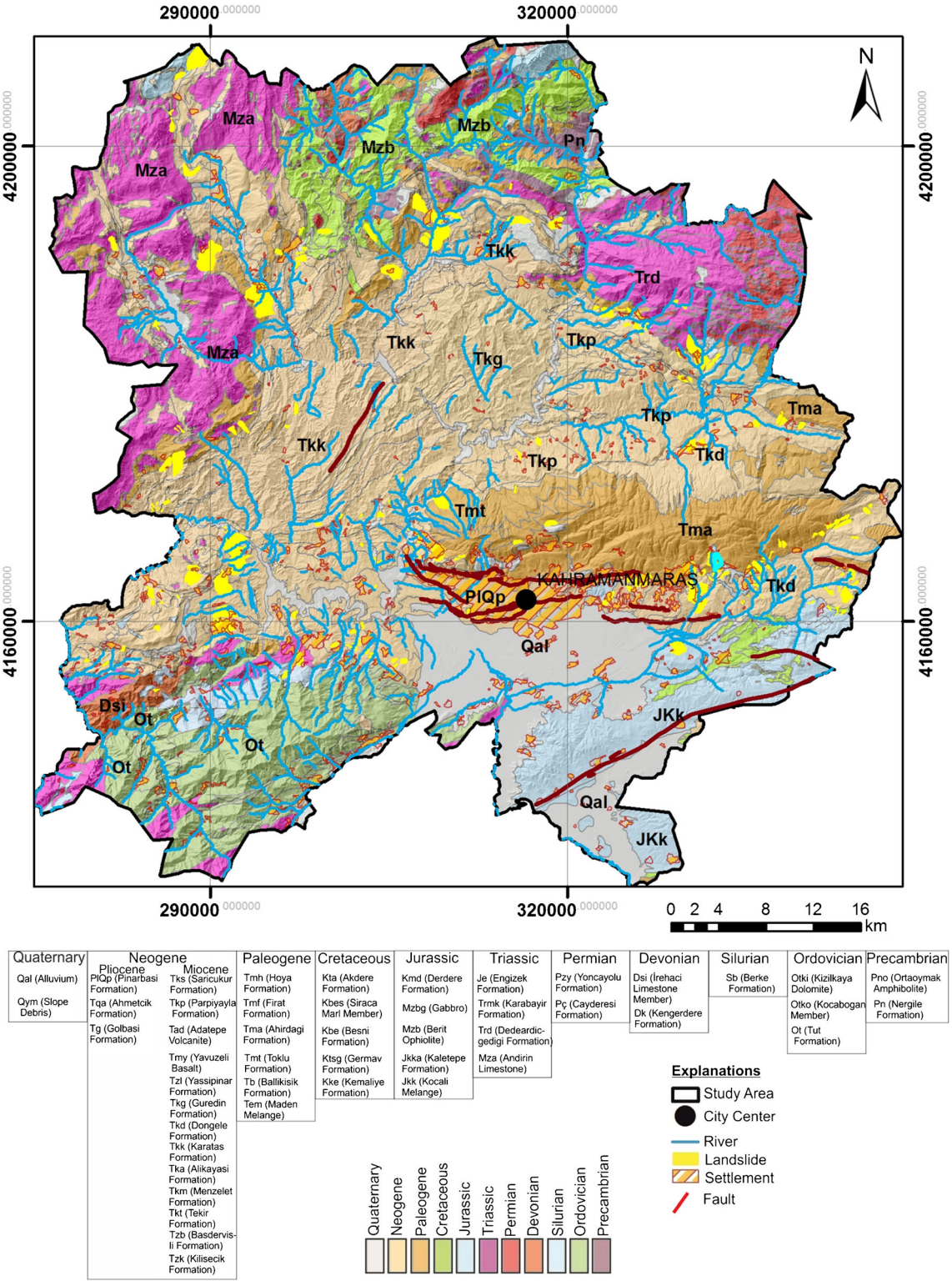

Fig. 2 Geological features of the study area

has been frequently performed in the scientific landslide literature. Basically, two approaches, qualitative and quantitative methods, have been adopted for the preparation of landslide susceptibility maps. Qualitative methods are generally carried out depending on the field observations by using the knowledge and experience of the researcher, while quantitative methods are performed by using statistical and/or mathematical modelling techniques. In quantitative methods, the

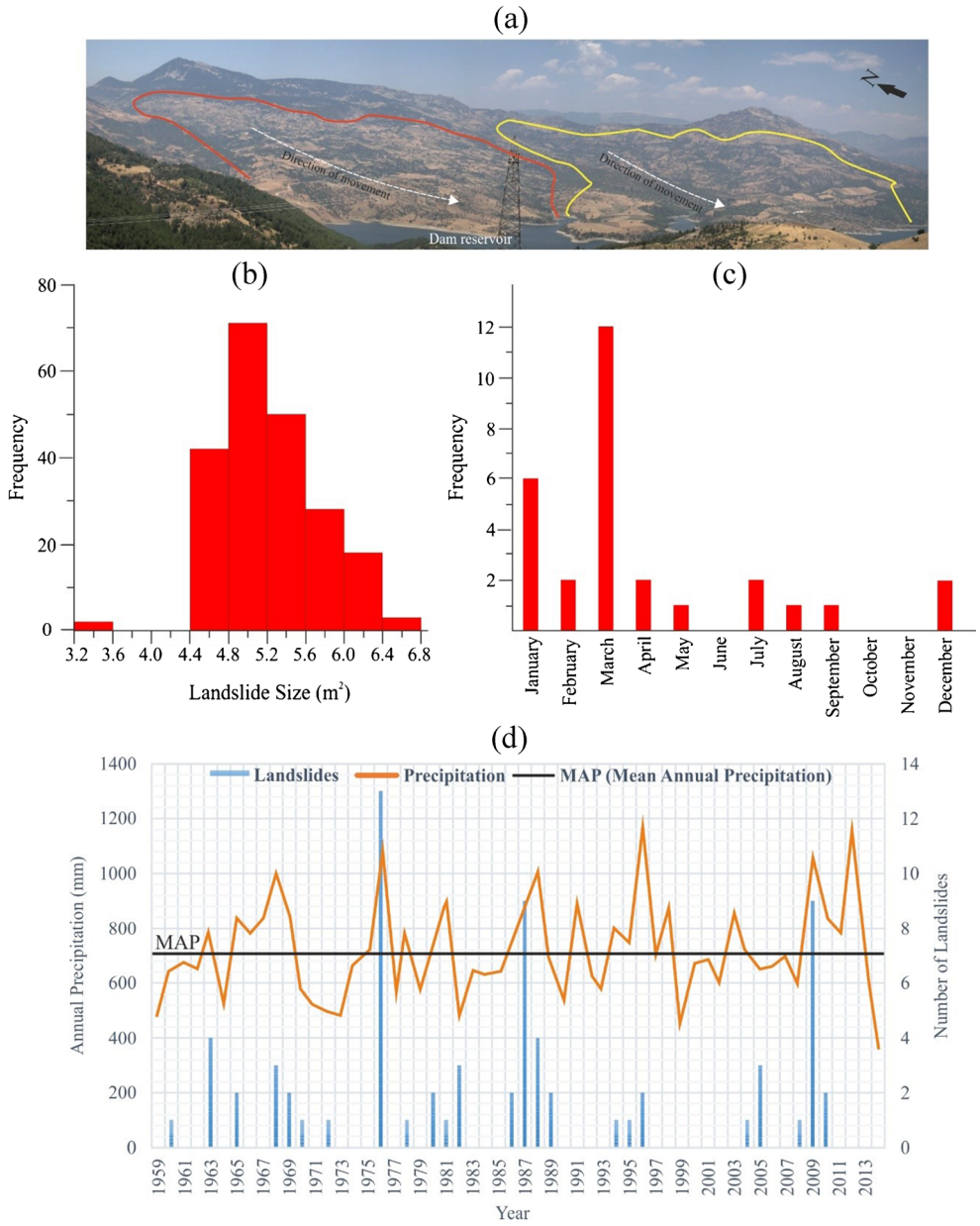

Fig. 3 Landslide features of the study area: **a** a view of the landslides, **b** frequency distribution of landslide sizes, **c** frequency distribution of landslide occurrence months and **d** annual precipitation of KMS and number of landslides in the study area

parameters that are related to landslides are statistically evaluated and are produced as digital maps, mostly on a GIS platform. For example, in addition to some multivariate statistical analyses, frequency ratio (FR), logistic regression (LR), support vector machines (SVM) and artificial neural networks (ANN) have been widely used to assess and/or to compare landslide susceptibility in many studies (Li et al. 2017; Chen et al. 2019a; Gholami et al. 2019). Although all these methodologies had pros and cons, we preferred to assess landslide susceptibility in the study area by FR and LR methods which were successfully applied in the landslide literature for different regions.

The FR method has been one of the most widely used and simple methodologies to evaluate and/or to compare the landslide-related factors and their relationships between the landslide and non-landslide locations (e.g. Solaimani et al. 2013; Mondal and Maiti 2013; Regmi et al. 2014; Meten et al. 2015; Youssef et al. 2015; Wang et al. 2016; Wu et al. 2016; Zhang et al. 2016a, 2016b; Chen et al. 2017; Li et al. 2017; Nicu 2017; Pirasteh and Li 2017b; Sahana and Sajjad 2017; Aditian et al. 2018; Mandal et al. 2018; Zhu et al. 2018; Arca et al. 2019; Jana et al. 2019; Nsengiyumva et al. 2019; Yan et al. 2019). Actually, the theory behind the FR method is a simple ratio of A (area of landslides in a parameter class to area of all landslides) to B (area of a parameter class to the entire area) (i.e. FR = A/B). The FR value greater than 1 reflects a strong relationship, while the FR value less than 1 presents a poor relationship between the landslides and the

considered parameters (Lee and Sambath 2006). Thus, landslide conditioning parameters were produced by the available data in a GIS platform to produce the landslide susceptibility map by the FR method. The considered parameters related to landslides in the region were slope (SLP), lithology (LIT), aspect (ASP), topographical elevation (TEL), distance to rivers (DTR), land use (LUS), curvature (CRV), distance to faults (DTF) and normalized difference vegetation index (NDVI). The SLP, ASP, TEL and CRV parameters were obtained from the digital elevation model (DEM) (containing 26,300,000 pixels) with the 10 m*10 m resolution, gathered from the General Directorate of Mapping of Turkey. The DTR map was produced from DEM using ArcHydro tools and GIS procedures. The LUS map was gathered from AFAD data, produced from Coordination of Information on the Environment (CORINE) codes. The NDVI map was produced from a Landsat ETM+ satellite image using red (R; band 3) and near-infrared (NIR; band 4) bands by rationing the reflectance values of the related bands (NDVI = (NIR − R) / (NIR + R)). In addition, the landslide inventory map (containing 805,662 pixels) was also integrated to the database in digital format. All files were stored in the GIS platform, and they are presented in Fig. 4. The next step of the FR analysis was to calculate the number of pixels either in the domain of a subgroup of a considered parameter or in the landslide inventory map. This calculation was made in the GIS platform, and the number of pixels related to the FR equation was extracted. Then, the FR values of the considered parameters and their subgroups were evaluated (Table 2). Finally, the Landslide Susceptibility Index (LSI) was calculated by the summation of FR values of each parameter as given below (Lee and Sambath 2006):

$$\mathrm{LSI} = \sum \mathrm{FR}\ \left(\text{FR rating of each factor's type or range}\right) \quad (1)$$

The landslide susceptibility map produced by FR was obtained (Fig. 5a) using the equation above and standardized in [0, 1] interval which ranges from very low to very high landslide susceptibility classes.

As for the LR method, it has also been one of the most commonly used methods for landslide susceptibility mapping purposes among the researchers in recent years (e.g. Talaei 2014; Bai et al. 2015; Lombardo et al. 2015; Chen et al. 2016; Sangchini et al. 2016; Wang et al. 2016; Du et al. 2017; Pham et al. 2017a, 2017b; Raja et al. 2017; Sahana and Sajjad 2017; Wu et al. 2017; Achour et al. 2018; Mandal and Mandal 2018; Polykretis and Chalkias 2018; Chen et al. 2019b; Kadavi et al. 2019; Soma et al. 2019). Conventionally, application of the LR method to produce a landslide susceptibility map is performed by dependent (landslide inventory) and independent variables (conditioning parameters of landslides) (Nandi and Shakoor 2009). LR analyses were performed by the LogisticReg module of the Idrisi Selva computer code. This module performs binomial logistic regression using raster or attribute values files. One of the most important advantages of the logistic regression method is that continuous and/or discrete variables could be used for the calculation stage (Lee and Sambath 2006). For the LR analyses, the dependent (i.e. landslide inventory) and 9 independent variables (slope, lithology, aspect, topographical elevation, distance to rivers, land use, curvature, distance to faults and normalized difference vegetation index) were loaded to the GIS platform. In the LR analysis, the module estimates a model of probability which represents the relationship between the dependent and independent variables. The probability of the dependent variable is calculated by the equation given below:

$$P(y = 1|X) = (\exp(\sum BX)/(1 + \exp(\sum BX)) \quad (2)$$

where P is the probability of the dependent variable being 1 (landslide); X is the independent variables (conditioning parameters) ($X = (x_0, x_1, x_2, \ldots, x_k)$ and B is the estimated coefficients of the considered input parameters ($B = (b_0, b_1, b_2, \ldots, b_k)$ (Eastman 2012). Then, a linearization process is needed to remove the zero and one boundaries for the probability of the dependent variable. By doing so, the predicted probability value (P') will range from 0 to 1 and will be continuous by applying Eq. 3 (Eastman 2012):

$$P' = \mathrm{Ln}(P/1-P) = \mathrm{b0} + \mathrm{b1}*\mathrm{x1} + \mathrm{b2}*\mathrm{x2} + \ldots\ldots + \mathrm{bk}*\mathrm{xk} + \mathrm{error} \quad (3)$$

In addition, the maximum likelihood estimation procedure is used in the related module of the computer code for finding the best-fitting set of independent parameters (Eastman 2012). These procedures are carried out by the following equations:

$$L = \prod_{i=1}^{N} \mu_i^{yi}\ x\ (1-\mu_i)^{(1-yi)} \quad (4)$$

$$\mu_i = \exp\left(\sum_{k=0}^{K} b_k x_{ik}\right) / \left(1 + \exp\left(\sum_{k=0}^{K} b_k x_{ik}\right)\right. \quad (5)$$

where L is the likelihood, μ_i corresponds to the predicted value of the dependent variable for sample i, N refers to the number of samples and y_i is the observed value of the dependent variable for sample i (Eastman 2012). A stratified random sampling strategy was applied for the analyses considering 10% sampling proportion by default. LogisticReg module also summarizes some statistical indicators such as − 2log(L0), − 2log(Likelihood) and pseudo R^2. These values indicate how well the model fit or not considering the parameters fed into the analyses. For example, pseudo R^2 values greater than 0.2 indicate a relatively good fit, and the model is assumed as

acceptable (Eastman 2012). The statistical results of LR are tabulated in Table 3, and the landslide susceptibility map produced by the LR model is shown in Fig. 5b. Since the pseudo R^2 value was greater than 0.2, the model was accepted as a relatively good fit.

The final stage of the landslide susceptibility mapping procedures was to assess the performance of the so-produced maps by FR and LR methods. It was conducted by the ROC module of Idrisi Selva. The ROC module calculates the area under the curve (AUC) value using true- and false-positive percentages for each class, and the user can draw the ROC curve using these percentages. The AUC value of 1 corresponds to a perfect fit, while the AUC value of 0.5 is considered as an agreement by chance. During this stage, 8,878,255 pixels (covering approximately 33% of the study area), which were allocated for this validation stage and were never used for the former FR and LR analyses, were taken into consideration. Thus, by using this module, AUC values were calculated for each susceptibility map. The values were 0.862 and 0.828 for FR and LR methods, respectively. The schematic representation of these results is shown in Fig. 5c. Although the AUC values were close to each other, the landslide susceptibility map produced by the FR method was selected as the input for the landslide hazard assessment because of its higher AUC value.

Landslide hazard

Similar to the landslide susceptibility assessments, landslide hazard mapping techniques are divided into two major groups such as qualitative (direct) and quantitative (indirect) methods. Qualitative methods are generally based on expert opinion and considered as subjective. On the contrary, quantitative methods are considered as objective and produce numerical estimates (probabilities) of the occurrence of landslide phenomena in any hazard zone (Guzzetti et al. 1999). For both cases, data quality, reliability and the completeness of the landslide database are the most significant items for hazard assessments. In addition, the hazard (H) component is by far the most complex to establish since it is almost impossible to link the temporal probability with the landslide occurrences due to the lack of reliable historical and complete landslide data in many parts of the world (Van Westen et al. 2006).

Incompleteness of the landslide inventory is one of the most important problems when one tries to produce a landslide hazard and/or risk map. Thus, it becomes almost impossible to reach the exact definition of hazard including the three components (spatial, temporal and magnitude/size probabilities) in many studies proposed by Guzzetti et al. (1999). Of these, the magnitude (i.e. size, volume, intensity, etc.) component was not considered for the landslide hazard stage in this study due to the incompleteness of the landslide database. This situation can also be confirmed in Fig. 3b, particularly for small landslide sizes covering a few thousand square metres of areal extent. In addition, information related to the triggering event(s) is also a problematic issue. One of the most important reasons for this difficulty is generally sourced from the absence of the documentation of landslide occurrences and triggering agents such as earthquake, rainfall, human activity, etc. Furthermore, triggering factors are peculiar to the area concerned, and their effects on the landslide occurrences may be different for each site.

Fig. 4 Parameter maps used in the susceptibility analyses: **a** aspect, **b** curvature, **c** distance to faults, **d** distance to rivers, **e** normalized difference vegetation index, **f** slope, **g** topographical elevation, **h** lithology and **i** land use

Given the problems mentioned above, landslide hazard assessment was conducted by the available data at hand. The first step of this assessment was to identify the triggering factor(s). Based on our archive studies and the interviews with local people during the field studies, the staple point of these works was that the precipitation was the major triggering factor of landslides. In addition, even if it was not valid for all landslides in the database, there was a good compatibility between the higher precipitation values and number of landslides represented in Fig. 3d. Therefore, precipitation was determined as the major triggering factor in the study area according to these studies. In these studies, there were no earthquake-triggered landslide data or damage information caused by landslides following an earthquake. However, the study area was located in a seismically active zone. In addition, as mentioned before, the Eastern Anatolian Fault Zone (EAFZ) and its segments are very close to the study area, particularly in the SE part (see Fig. 2). Thus, instead of not eliminating earthquake as a triggering factor of landslide occurrences, it was used as a hazard component. For this stage, the approaches provided by Abella and Van Westen (2007) and Akgun et al. (2012) were considered although there were no earthquake-triggered landslide data in their database. In these studies, peak ground acceleration (PGA) was taken into consideration as a triggering indicator with respect to landslide hazard. For this purpose, an index map (LHI) was produced by using Eq. 6 and Eq. 7:

$$\mathrm{LHI} = \mathrm{LSI}*\mathrm{TI} \tag{6}$$

$$\mathrm{TI} = (\mathrm{PGA}*0.2) + (\mathrm{PRE}*0.8) \tag{7}$$

where LHI is the landslide hazard index, LSI refers to the landslide susceptibility index and TI is the triggering indicator of landslides including precipitation (PRE) and PGA data. Of these, LSI was obtained in the previous section. For the triggering indicators, PGA and PRE maps were used as inputs of TI. For the PGA map, earthquake hazard map of the study area was gathered from AFAD. It was based on PGA values

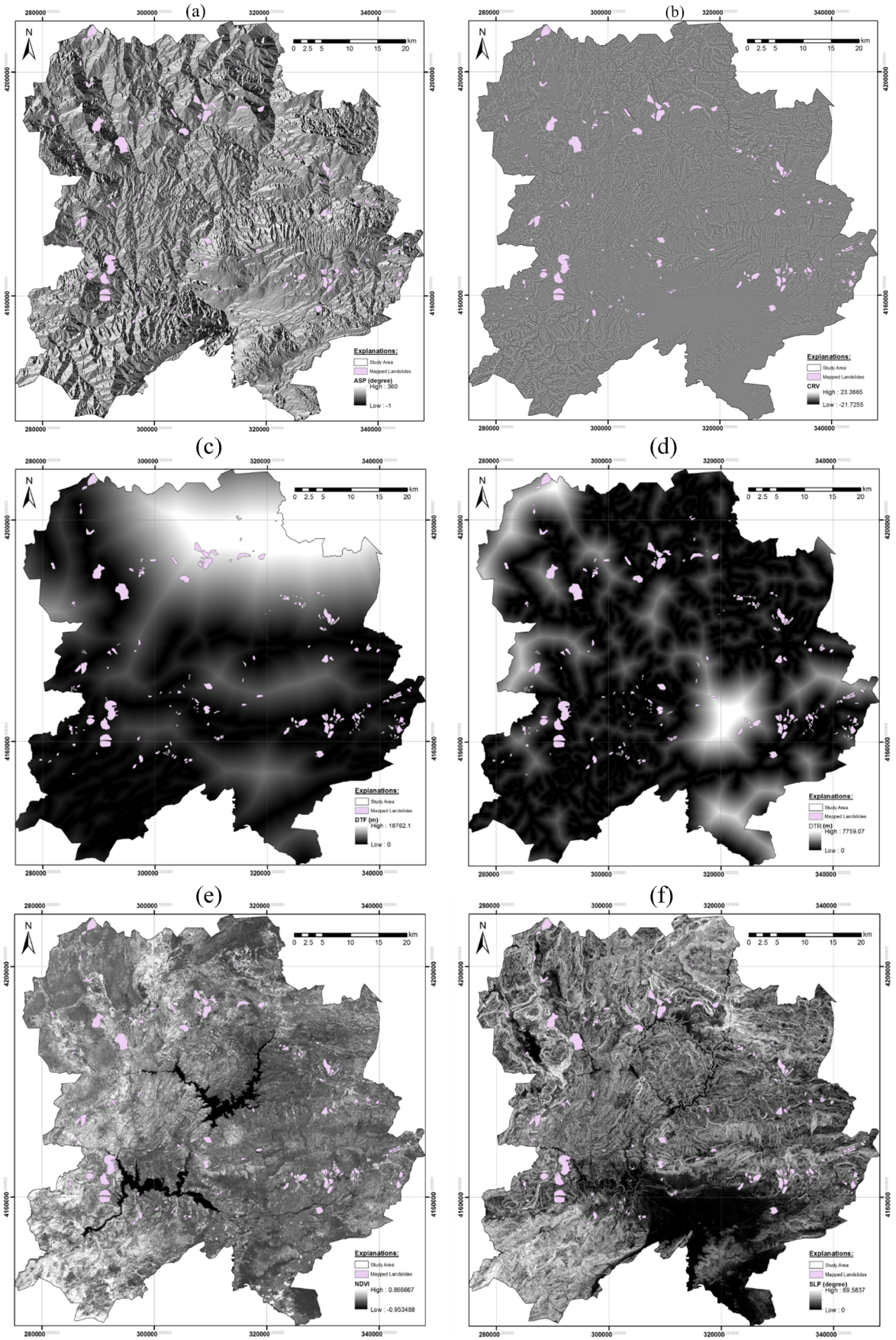
(a)
(b)
(c)
(d)
(e)
(f)
N
0 2.5 5 10 15 20 km
280000 300000 320000 340000
4200000 4160000 4100000
Explanations:
Study Area
Mapped Landslides
ASP (degree)
High : 360
Low : -1
CRV
High : 23.3665
Low : -21.7255
DTF (m)
High : 18762.1
Low : 0
DTR (m)
High : 7759.07
Low : 0
NDVI
High : 0.866667
Low : -0.953488
SLP (degree)
High : 69.5837
Low : 0

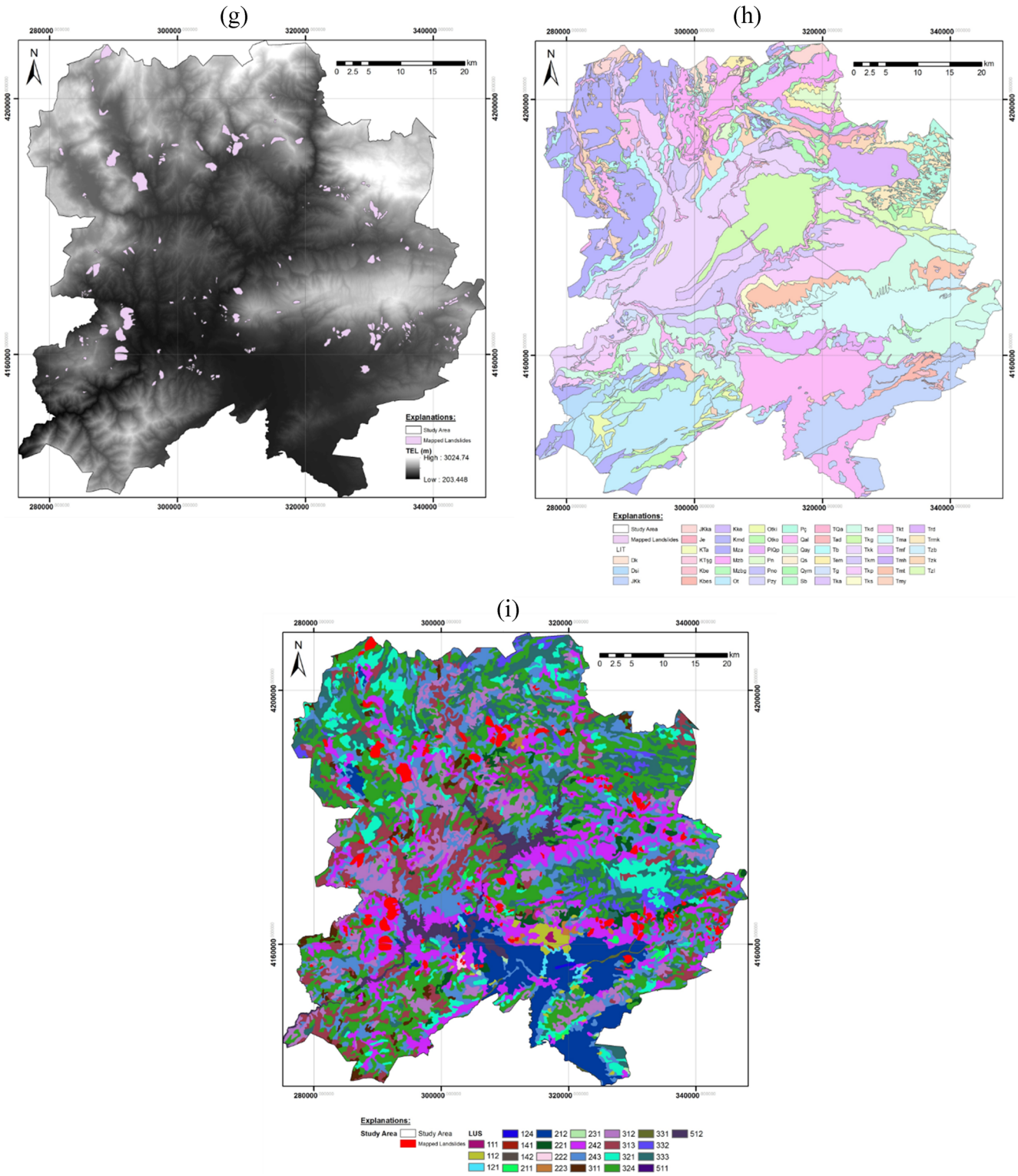

Fig. 4 (continued)

ranging from very low to very high hazard, which corresponds to 10% probability of exceedance in 50 years with a return period of 475 years. This map was standardized in [0, 1] interval for the study area and is shown in Fig. 6a as an input of TI. Then, the other input of TI, namely the PRE map, was produced. To produce the PRE map of the study area, the approach provided by Akgun et al. (2012) was considered. Data scarcity and deficiency problems related to the

Table 2 FR values of the considered parameters and their subgroups

ASP (°)	# of pixels in domain (A)	# of pixels in landslided areas (B)	FR	DTR (m)	# of pixels in domain (A)	# of pixels in landslided areas (B)	FR
N (0–22.5; 337.5–360)	2,315,742	97,046	1.37	0–250	5,284,976	249,277	1.54
NE (22.5–67.5)	2,736,079	125,042	1.49	250–500	4,275,524	219,445	1.67
E (67.5–112.5)	3,169,091	134,151	1.38	500–750	3,214,754	103,894	1.05
SE (112.5–157.5)	3,448,359	133,082	1.26	750–1000	2,433,983	73,337	0.98
S (157.5–202.5)	3,955,951	107,591	0.89	1000–1250	1,887,945	46,177	0.79
SW (202.5–247.5)	3,718,105	81,163	0.71	1250–1500	1,487,251	29,291	0.64
W (247.5–292.5)	3,573,060	86,197	0.79	1500–1750	1,149,370	20,729	0.59
NW(292.5–337.5)	3,355,835	41,390	0.40	1750–2000	952,159	18,675	0.64
Flat (− 1)	27,778	0	0.00	2000–2500	1,465,419	44,052	0.98
CRV				2500–3000	1,163,715	785	0.02
<− 2.8	285,181	7382	0.84	> 3000	2,984,904	0	0.00
(− 2.8) to (− 1.8)	985,377	34,314	1.14	TEL (m)			
(− 1.8) to (− 0.8)	3,400,784	196,043	1.88	0–500	1,708,583	10,369	0.19
(− 0.8) to (− 0.3)	3,809,495	119,981	1.03	500–750	5,347,207	150,590	0.92
(− 0.3) to (0.2)	7,856,450	253,717	1.05	750–1000	4,799,825	235,085	1.59
(0.2)–(0.7)	4,609,160	119,708	0.85	1000–1250	3,989,234	205,928	1.68
(0.7)–(1.7)	4,070,563	46,284	0.37	1250–1500	3,340,579	140,199	1.37
(1.7)–(2.7)	983,552	23,950	0.79	1500–1750	2,904,217	40,916	0.46
(> 2.7)	299,438	4283	0.47	1750–2000	2,401,193	17,967	0.24
DTF (m)				2000–2250	1,185,807	4608	0.13
0–1000	8,097,279	420,925	1.69	2250–2500	423,439	0	0.00
1000–2000	4,344,442	201,967	1.52	2500–2750	182,113	0	0.00
2000–3000	2,922,922	68,777	0.77	>2750	17,803	0	0.00
3000–4000	2,230,188	46,559	0.68	SLP (°)			
4000–5000	1,708,301	26,413	0.50	(0–5)	3,176,603	0	0.00
5000–6000	1,057,217	10,884	0.34	(5–10)	2,651,230	153,564	1.89
6000–7000	643,305	12,003	0.61	(10–15)	3,399,132	184,827	1.77
7000–8000	583,376	14,497	0.81	(15–20)	4,051,355	183,798	1.48
8000–9000	552,300	3637	0.21	(20–25)	4,168,157	137,530	1.07
9000–10,000	546,517	0	0.00	(25–30)	3,805,374	83,657	0.72
>10,000	3,614,153	0	0.00	(30–35)	2,816,728	42,868	0.49
NDVI				(> 35)	2,231,421	19,418	0.28
(<− 0.4)	19,358	585	0.98	LUS (*)			
(− 0.4 to 0.2)	559,954	2577	0.15	111	17,094	0	0.00
(− 0.2 to 0.0)	7,310,931	160,951	0.72	112	192,066	0	0.00
(0.0 to 0.2)	13,592,953	439,879	1.05	121	56,790	0	0.00
(0.2 to 0.4)	3,997,792	201,670	1.64	124	10,965	0	0.00
(> 0.4)	819,012	0	0.00	141	3422	0	0.00
LIT				142	2096	0	0.00
Otki	172,031	0.00	0.00	211	83,709	3168	1.23
Otko	173,944	0.00	0.00	212	1,737,347	16,387	0.31
JKk	1,329,095	19,143	0.47	221	359,761	9016	0.82
Mza	2,552,727	35,197	0.45	222	14,607	2169	4.85
Ot	1,576,820	13	0.00	223	61,686	5909	3.13
Kmd	9029	0	0.00	231	20,806	153	0.24
Tmy	89,585	48	0.02	242	3,500,267	412,563	3.85
Sb	223,208	4260	0.62	243	4,283,610	158,580	1.21
Dk	140,954	0	0.00	311	330,345	7180	0.71

Table 2 (continued)

ASP (°)	# of pixels in domain (A)	# of pixels in landslided areas (B)	FR	DTR (m)	# of pixels in domain (A)	# of pixels in landslided areas (B)	FR
Tkk	2,814,592	155,387	1.80	312	2,067,798	10,655	0.17
Mzbg	27,848	0	0.00	313	2,276,898	45,609	0.65
Qal	2,211,679	0	0.00	321	1,511,866	5119	0.11
Pç	545,778	949	0.06	324	6,002,138	97,239	0.53
Pzy	62,371	0	0.00	331	37,465	0	0.00
Tzk	518,234	26,166	1.65	332	449,989	596	0.04
Qym	399,732	6491	0.53	333	2,637,030	31,209	0.38
Tkp	1,706,134	66,334	1.27	511	5594	110	0.64
Tem	217,809	3070	0.46	512	636,651	0	0.00
Tb	760,527	73,961	3.17				
Trd	578,491	2113	0.12				
Mzb	1,167,800	13,221	0.37				
Pn	198,875	479	0.08				
Tad	37,625	1065	0.92				
Tkm	877,520	20,727	0.77				
Tka	308,251	3414	0.36				
Jkka	149,144	0.00	0.00				
Tzl	302,848	23,959	2.58				
Qs	18,299	0	0.00				
Tkg	1,076,819	59	0.00				
TQa	16,052	0	0.00				
Pno	74,163	0	0.00				
Tkd	2,035,269	226,461	3.63				
PlQp	377,691	10,175	0.88				
Tg	293,172	18,761	2.09				
Trmk	380,990	6106	0.52				
Tma	1,555,772	56,006	1.17				
Kke	2748	0	0.00				
Tkt	119,378	8574	2.34				
Je	120,008	1200	0.33				
Tzb	84,919	0	0.00				
Kbe	57,726	0	0.00				
KTa	51,475	0	0.00				
Tks	89,687	4632	1.69				
Tmf	17,743	992	1.83				
Dsi	179,990	929	0.17				
Tmt	454,624	15,078	1.08				
Ktşg	13,486	692	1.68				
Kbes	109,751	0	0.00				
Tmh	4342	0	0.00				
Qay	13,245	0	0.00				

**Explanations for CORINE codes:* 111, continuous urban fabric; 112, discontinuous urban fabric; 121, industrial or commercial units; 124, airports; 141, green urban areas; 142, sport and leisure facilities; 211, non-irrigated arable land; 212, permanently irrigated land; 221, vineyards; 222, fruit trees and berry plantations; 223, olive groves; 231, pastures; 242, complex cultivation patterns; 243, land principally occupied by agriculture, with significant areas of natural vegetation; 311, broad-leaved forest; 312, coniferous forest; 313, mixed forest; 321, natural grasslands; 324, transitional woodland-shrub; 331, beaches, dunes, sands; 332, bare rocks; 333, sparsely vegetated areas; 511, water courses; 512, water bodies

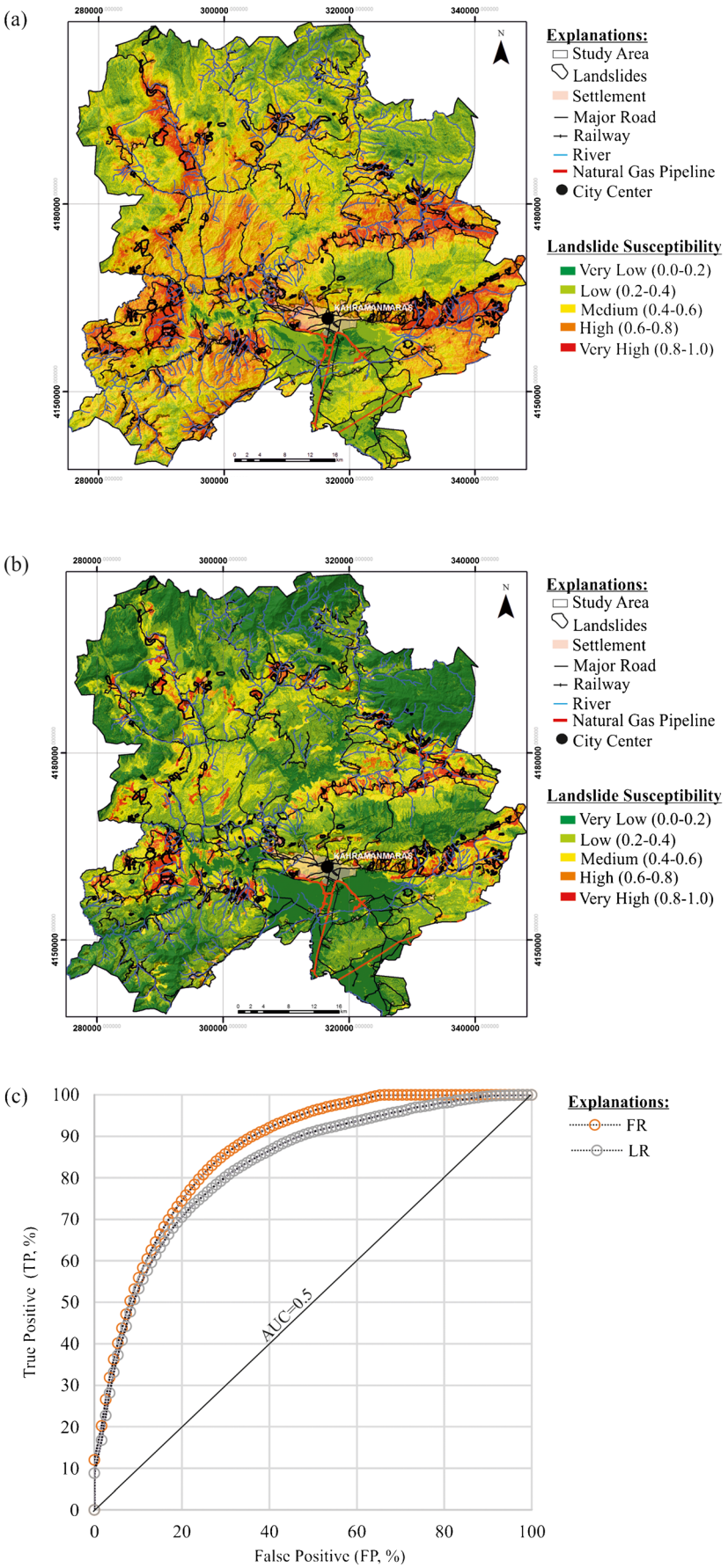

Fig. 5 Landslide susceptibility analysis results: **a** FR map, **b** LR map and **c** ROC curves

precipitation and landslide data were almost the same in their study area. For this reason, we considered the additional data of three meteorological stations (Göksun, Afşin and Elbistan; for the locations, see Fig. 1) at which the most long-term data exist regardless of their deficiencies in some years, along with the data of KMS. Thus, considering the annual precipitation data of these four meteorological stations from 1959 to 2014, the PRE map was obtained by using the inverse distance weighted technique. This map was standardized for the study area similar to the PGA indicator and is shown in Fig. 6b as a second input of TI. Then, to produce the LHI map, PGA and PRE maps were multiplied by 0.2 and 0.8, respectively, as suggested by Abella and Van Westen (2007). In other words, the TI part of LHI was obtained by using Eq. 7. Finally, the LHI map of the study area was produced (Fig. 7) using these equations. The LHI map was classified into five groups ranging from very low (1) to very high (5) classes to represent the hazard component of the LRI.

Vulnerability

Losses and/or damages that may be raised from any natural disaster should be evaluated by considering economic, social, socio-economic or environmental factors. Based on the literature studies, scientists generally considered vulnerability part of landslide risk in four different groups such as physical, economic, environmental and social ones. Naturally, the most important element is human life, but it is suggested that other factors should also be taken into consideration (Fell et al. 2008a, 2008b). It is evident that an interdisciplinary study is needed to evaluate this issue in a way that involves many different disciplines for a sustainable risk assessment and management. Vulnerability assessment is an essential part of the landslide risk evaluations (Bednarik et al. 2012). In addition, vulnerability assessment involves the understanding of the interaction between a given landslide and the affected elements (Dai et al. 2002). However, studies related to vulnerability with respect to landslides are far less abundant (Galli and Guzzetti 2007). Furthermore, it should be noted that there is a considerable amount of uncertainty in the vulnerability assessment stage. Thus, in many cases, researchers have to make some assumptions depending on factors such as scale, spatial features, data groups at hand, data quality and reliability.

In the literature, the term vulnerability was defined in many ways for various purposes. In addition to the definition of vulnerability given in the first section of this study by Varnes and IAEG (1984), it is possible to find out different definitions of vulnerability. Recent reviews and applications of vulnerability in different disciplines can be found in detail in Gonçalves and Zezere (2018), Behera et al. (2019), Giannakidou et al. (2019), Miranda and Ferreira (2019), Rehman et al. (2019) and Singh et al. (2019a, 2019b). From a different point of view, Köhle et al. (2007) considered vulnerability as a dynamic parameter in risk assessments since it has temporal and spatial content. Since it was almost impossible to access the data on temporal content for such a big area and there were many data deficiencies, the spatial content of vulnerability was solely considered by the available data of concern.

Similar to the absence of documentation problem between landslide occurrences and triggering factors mentioned in the hazard section, there are also problems arising from the lack of information between reliable and/or available damage data and landslides. To some extent, this situation also makes quantitative landslide risk assessments impossible (Van Westen et al. 2006). In addition, lack of damage data also hampered to produce vulnerability curves or functions as well as fragility curves. Therefore, it is one of the most challenging tasks to assess vulnerability as a part of risk concept when historical catalogues related to damage data for landslides are lacking, as in the case of this study.

To cope with these issues mentioned above, some indices were used in the literature, particularly for small- and medium-scale studies (e.g. Abella and Van Westen 2007; Akgun et al. 2012; Giannakidou et al. 2019). In this study, for the reasons mentioned above, it was preferred to produce a relative vulnerability index (RVI), as a second component of LRI, in addition to LHI. It contains mainly three different components such as environmental, infrastructural and population density features, based on the available data for the study area. In addition to RVI, its sub-components were also explained in the following lines.

In the study area, categorical land use (Fig. 8), water channels (WCH), potable water pipeline (PWP), power lines (PWL), road network (RON), railway (RAI) and natural gas pipeline (NGP) (Fig. 9) and population density data (Fig. 10)

Table 3 Statistical results of the LR method of landslide susceptibility analyses

Variables	Coefficient
Intercept	− 7.47
DTR	0.09
LUS	2.34
ASP	0.85
CRV	0.12
DTF	0.18
LIT	1.61
NDVI	0.54
SLP	0.81
TEL	1.15
− 2Log (L0)	768,953.77
− 2Log (L)	599,704.31
Pseudo R^2	0.22
χ^2 (9)	169,249.46

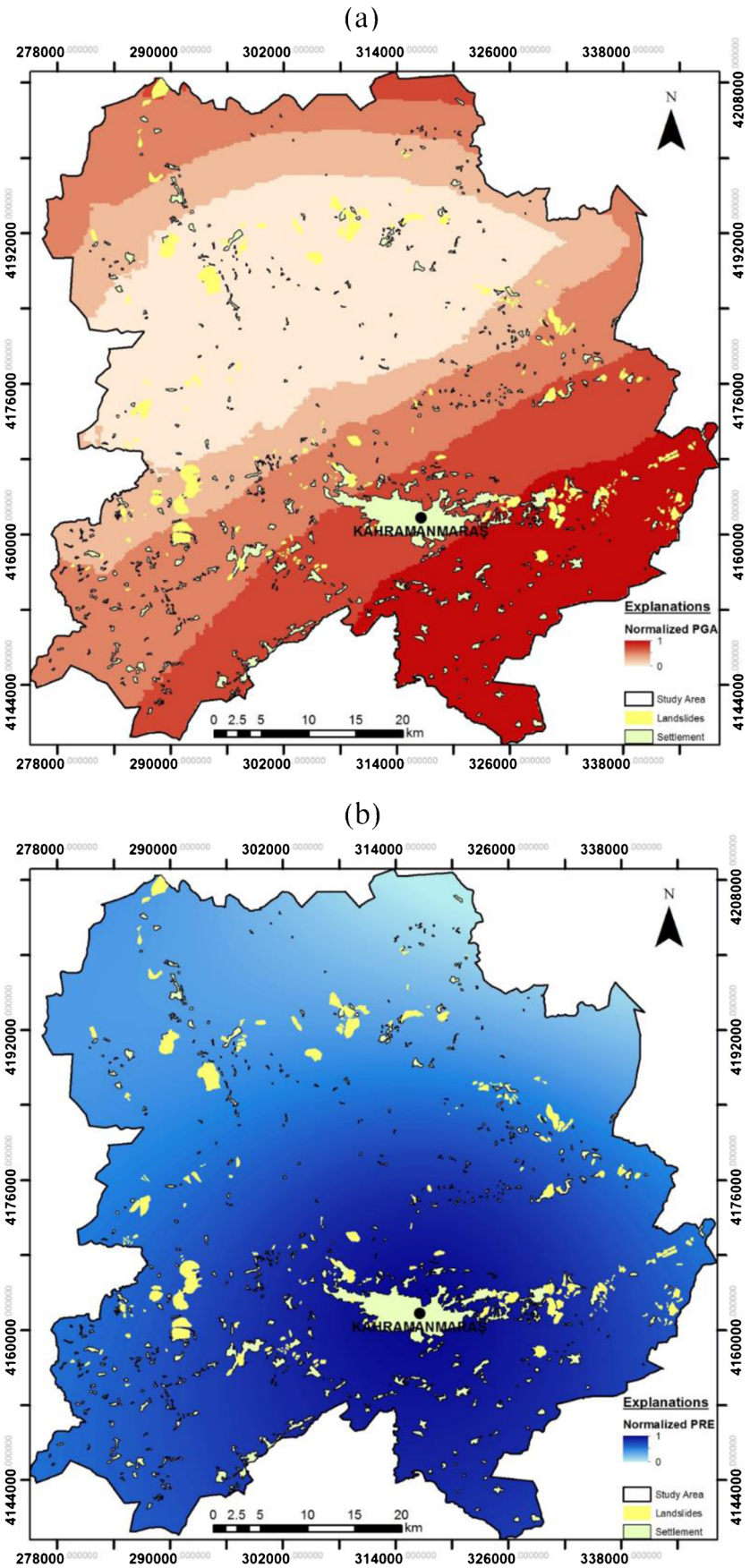

Fig. 6 Triggering factor maps of the study area: **a** PGA map and **b** PRE map

were taken into consideration as the elements at risk. All these data were gathered from the AFAD Provincial Directorate of Kahramanmaraş, based on the year of 2015 data. For land use components (see Fig. 4i and Table 2), they were classified into six groups (see Fig. 8) such as urban areas, plantation, agricultural, forest, bare land and water based on their categorical features for the AHP analyses explained below to shorten the number of parameters. In addition, linear density calculations (per km^2) were performed in the ArcGIS platform for lineament features of WCH, PWP, PWL, RON, RAI and NGP elements in the study area, and they were standardized in [0, 1] interval (see Fig. 9). For the population density (see Fig. 10), 2015 population density data of Kahramanmaraş were interpolated and standardized in [0, 1] interval throughout the study area.

As being a part of the specific risk, the term vulnerability depends basically upon the degree of loss (economically and/or physically) for the element(s) at risk and the magnitude/intensity (velocity, volume, energy, impact pressure, etc.) of a natural phenomenon (i.e. landslide in this case). In the scientific literature, some excellent reviews and applications can be found with respect to landslide vulnerability considering the loss and magnitude components (e.g. Leone et al. 1996; Catani et al. 2005; Galli and Guzzetti 2007; Totsching and Fuchs 2013; Bianchini et al. 2017; Singh et al. 2019a, 2019b). Due to the lack of such vulnerability-related data, vulnerability assessment was performed by considering the relative loss (RL) and spatial impact (SI) of the elements at risk in the study area to produce a RVI map (Fig. 11). In other words, degree of loss and magnitude and/or intensity components of vulnerability were simulated by RL and SI, respectively (see Fig. 11). Economic valuation (i.e. relative cost of the elements) of RL for environmental and infrastructural elements at risk was achieved by AHP matrices fulfilled by the

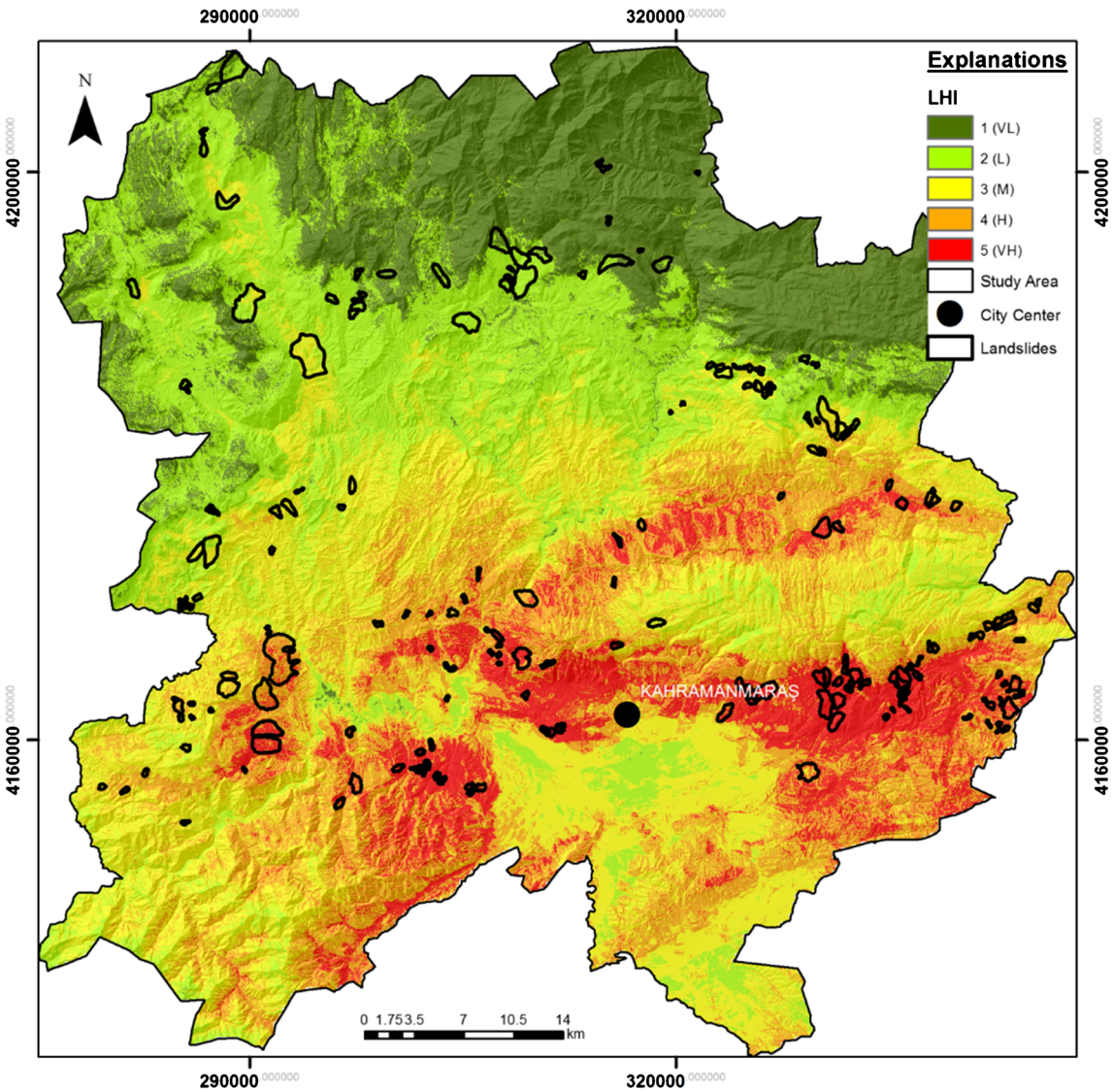

Fig. 7 LHI map of the study area

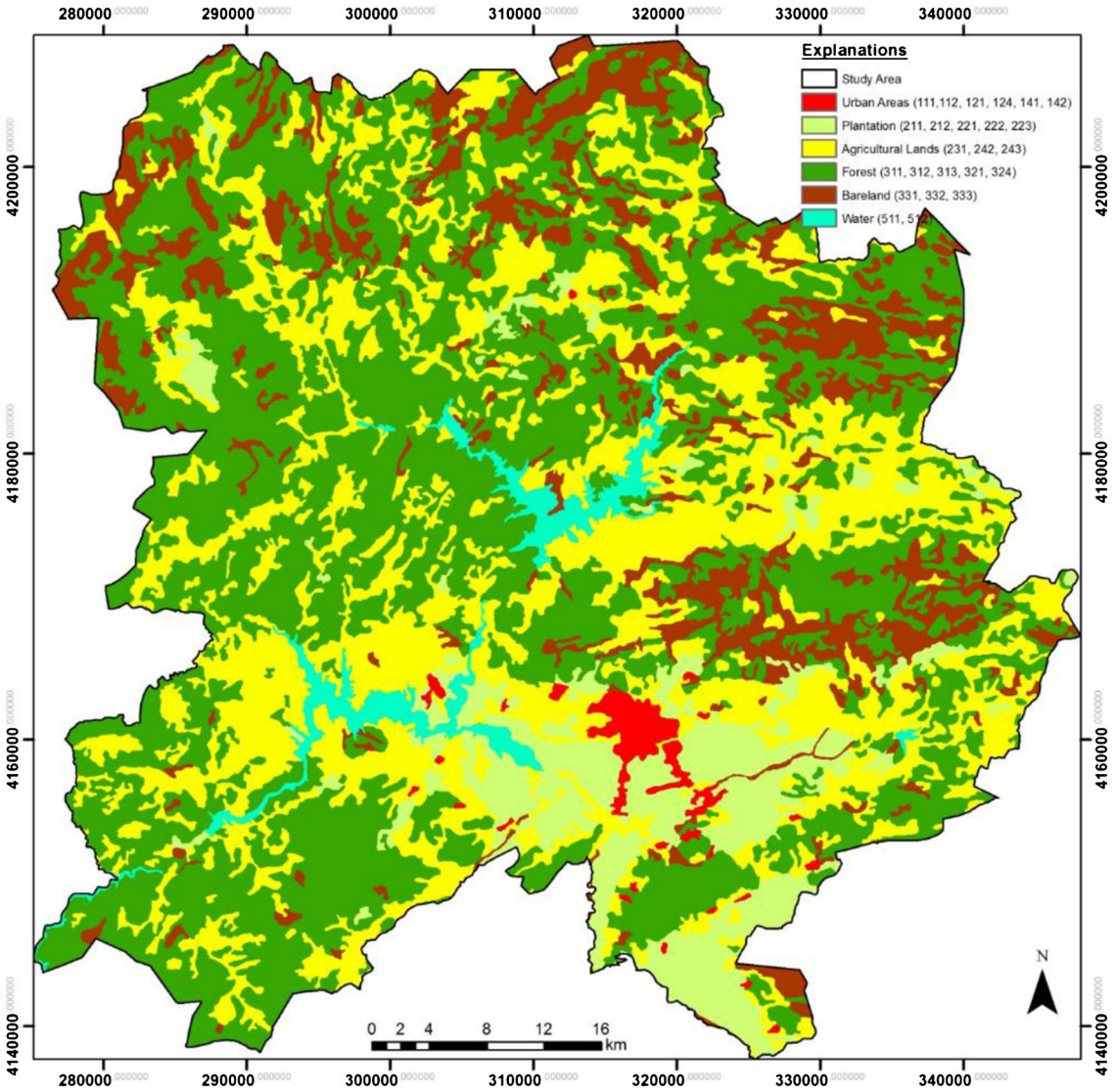

Fig. 8 Categorical land use map of the study area

local experts of AFAD. The question of "if a landslide occurs in the study area, what would be the relative economic loss on an element at risk because of this landslide?" was asked to these experts. For population data, a standardized population density map was used for RL. The spatial impact (SI) of the elements at risk was linked to the spatial distributions of these elements on the landslide locations based on categorical (for land use) and frequency distributions (for infrastructures and population) throughout the study area. SI values were simply calculated by dividing the number of pixels of each subgroup of element at risk to the total number of landslided pixels, expressed as landslide frequency (LF) in Fig. 11. The idea behind this concept was that the LF value of an element at risk would be high in the landslide areas if it was really linked to a landslide occurrence. If not, it would be low or zero as in the case of RAI and NGP components of infrastructural elements (see Fig. 11).

For the RL component, the AHP model was used for environmental and infrastructural vulnerability. The AHP method was introduced by Saaty (1977), and it was one of the most commonly used methods to cope with various problems in decision making. AHP is a theory of measurement through pairwise comparisons and relies on the judgements of experts to derive priority scales in relative terms (Saaty 2008). The reasons why we selected AHP theory to assess the RL component of vulnerability are mainly twofold: firstly, damage/loss data scarcity throughout the study area and, secondly, scale and size of the study area. Information such as economic loss and damage that may occur as a result of the landslides on the vulnerability of each element at risk could not be reached and/or was not available for the study area. Under these conditions, the most important advantage of the utilization of the AHP method was that it allowed the spatial expression of the RL to the elements at risk. To make comparisons, a scale of

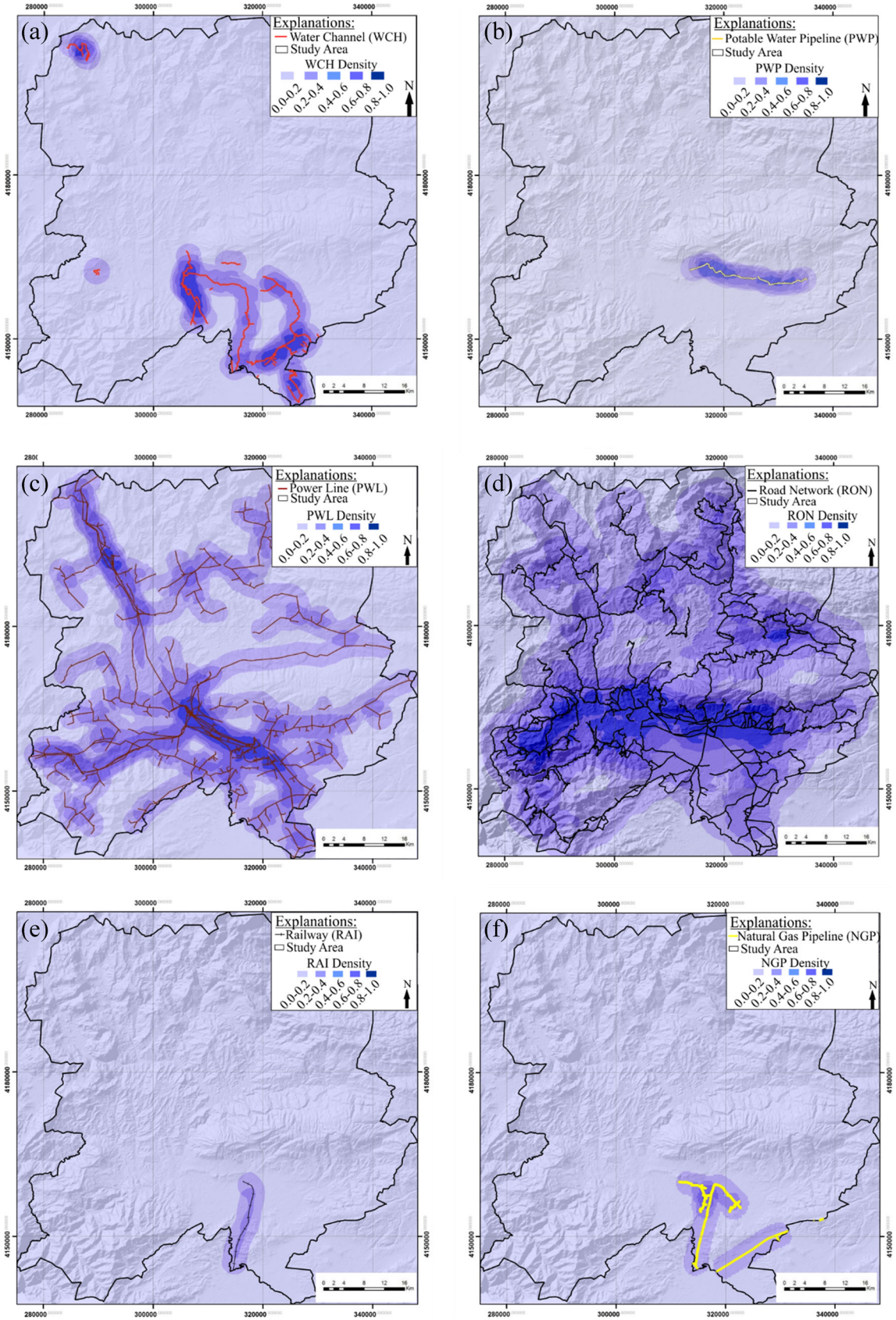

Fig. 9 Infrastructural elements-at-risk maps and their densities: **a** water channel, **b** potable water pipeline, **c** power line, **d** road network, **e** railway and **f** natural gas pipeline

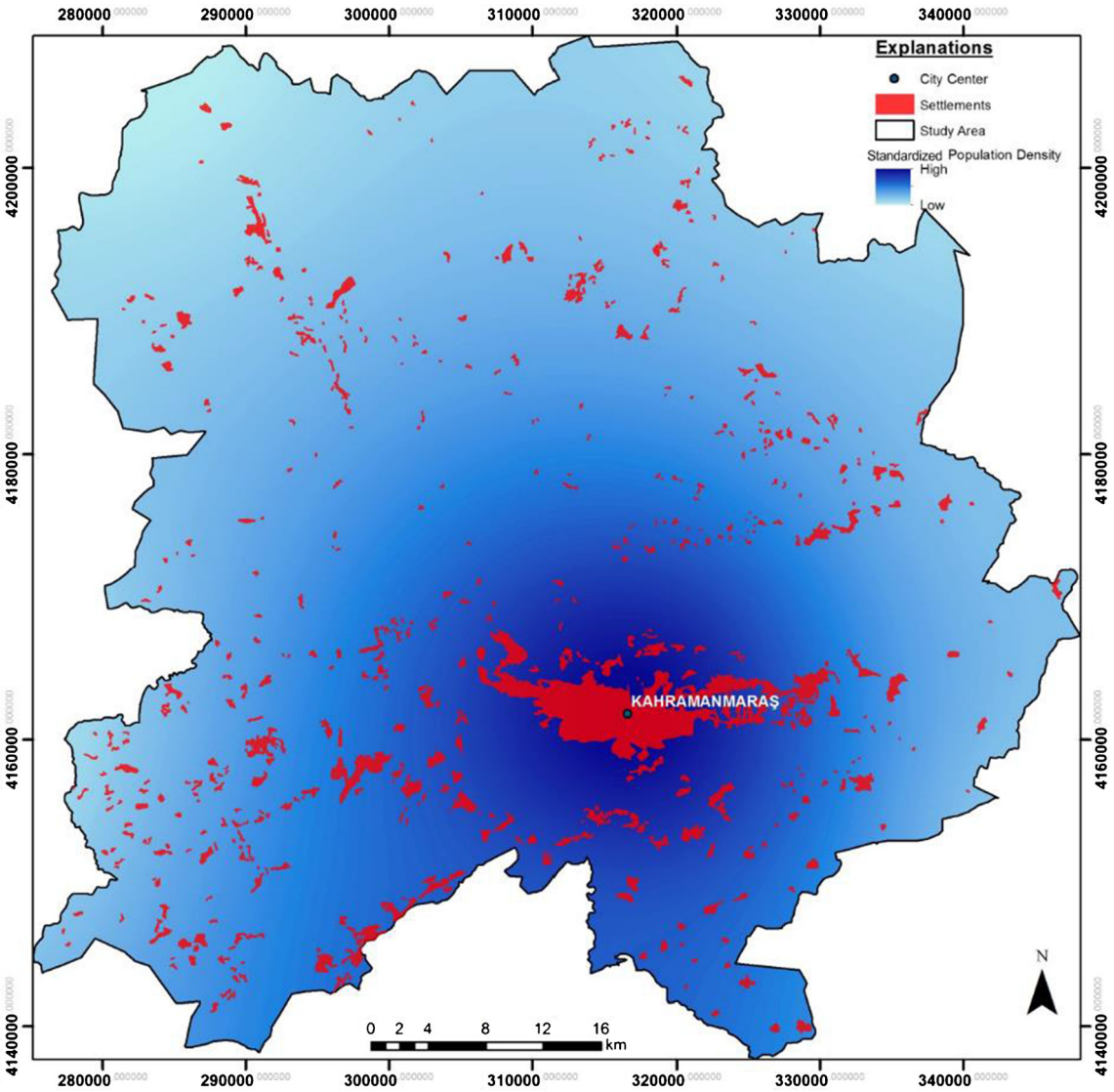

Fig. 10 Standardized population density map of the study area

numbers was needed, which indicated the importance among the elements (Saaty 2008). The scale provided by Saaty (1977) ranges between 1 (equal importance) and 9 (extreme importance), and the reciprocals (e.g. 1/9, 1/7, 1/3, etc.) could also be used when comparing the importance of the pairs to fulfil the AHP matrices. From this point of view, three local experts of AFAD were asked the question mentioned above to fulfil the AHP matrices for environmental and infrastructural elements at risk to achieve the RL component of the vulnerability. AHP matrices used to produce RL maps of the environmental and infrastructural elements at risk are tabulated in Table 4 and Table 5, respectively. The grey-shadowed parts in these tables correspond to the reciprocals of the values. To produce the RL maps, the considered elements-at-risk parameters of concern were fed into the GIS platform. For this stage, the weight module of the Idrisi Selva computer code was used. The module gives the value of consistency ratio (CR) as a measure of the consistency among the considered parameters. The CR value lower than 0.1 is acceptable with respect to the consistency of the parameters of concern (Saaty 1977). Details related to the AHP method can be found in Saaty (1977, 2008). As can be seen from Table 4 and Table 5, CR values were lower than 0.1, and they were considered as consistent. To obtain an RVI map of the study area, SI and RL components were multiplied and standardized in [0, 1] interval for each element-at-risk group in the GIS platform. Then, environmental (EVM), infrastructural (IVM) and population (PVM) vulnerability maps were obtained by these calculations. All these stages are represented in Fig. 11. EVM, IVM and PVM maps are also shown in Fig. 12a–c as the components of the RVI map. Finally, the RVI map of the study area (Fig. 12d) was produced by arithmetically adding these three vulnerability maps using the equations given below. It was classified in 5

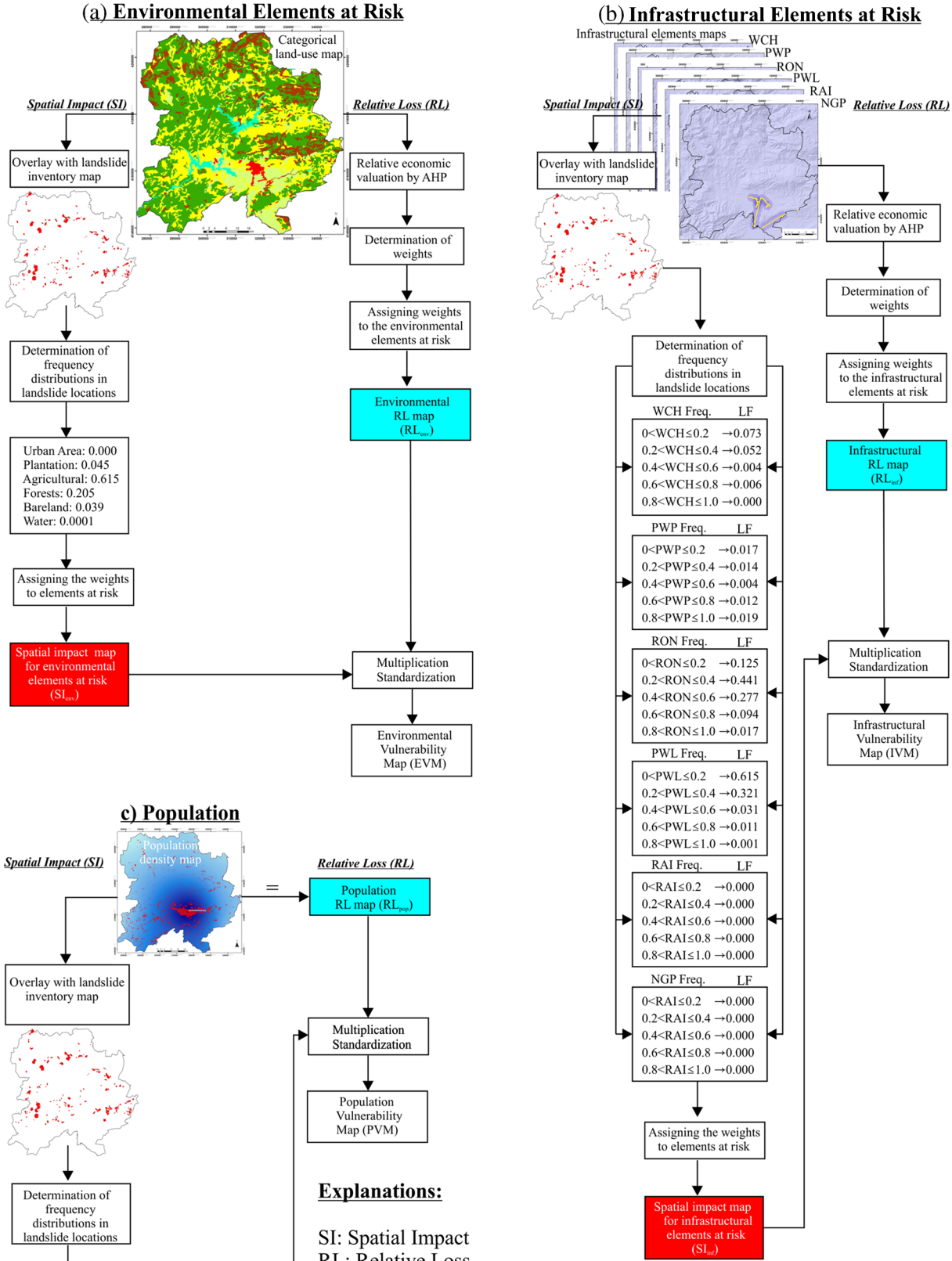
(a) Environmental Elements at Risk
Categorical land-use map
Spatial Impact (SI)
Relative Loss (RL)
Overlay with landslide inventory map
Relative economic valuation by AHP
Determination of weights
Assigning weights to the environmental elements at risk
Environmental RL map (RLenv)
Determination of frequency distributions in landslide locations
Urban Area: 0.000
Plantation: 0.045
Agricultural: 0.615
Forests: 0.205
Bareland: 0.039
Water: 0.0001
Assigning the weights to elements at risk
Spatial impact map for environmental elements at risk (SIenv)
Multiplication Standardization
Environmental Vulnerability Map (EVM)
(b) Infrastructural Elements at Risk
Infrastructural elements maps
WCH
PWP
RON
PWL
RAI
NGP
Spatial Impact (SI)
Relative Loss (RL)
Overlay with landslide inventory map
Relative economic valuation by AHP
Determination of weights
Assigning weights to the infrastructural elements at risk
Infrastructural RL map (RLinf)
Determination of frequency distributions in landslide locations
WCH Freq. LF
0<WCH≤0.2 →0.073
0.2<WCH≤0.4 →0.052
0.4<WCH≤0.6 →0.004
0.6<WCH≤0.8 →0.006
0.8<WCH≤1.0 →0.000
PWP Freq. LF
0<PWP≤0.2 →0.017
0.2<PWP≤0.4 →0.014
0.4<PWP≤0.6 →0.004
0.6<PWP≤0.8 →0.012
0.8<PWP≤1.0 →0.019
RON Freq. LF
0<RON≤0.2 →0.125
0.2<RON≤0.4 →0.441
0.4<RON≤0.6 →0.277
0.6<RON≤0.8 →0.094
0.8<RON≤1.0 →0.017
PWL Freq. LF
0<PWL≤0.2 →0.615
0.2<PWL≤0.4 →0.321
0.4<PWL≤0.6 →0.031
0.6<PWL≤0.8 →0.011
0.8<PWL≤1.0 →0.001
RAI Freq. LF
0<RAI≤0.2 →0.000
0.2<RAI≤0.4 →0.000
0.4<RAI≤0.6 →0.000
0.6<RAI≤0.8 →0.000
0.8<RAI≤1.0 →0.000
NGP Freq. LF
0<RAI≤0.2 →0.000
0.2<RAI≤0.4 →0.000
0.4<RAI≤0.6 →0.000
0.6<RAI≤0.8 →0.000
0.8<RAI≤1.0 →0.000
Assigning the weights to elements at risk
Spatial impact map for infrastructural elements at risk (SIinf)
Multiplication Standardization
Infrastructural Vulnerability Map (IVM)
c) Population
Spatial Impact (SI)
Population density map
=
Relative Loss (RL)
Population RL map (RLpop)
Overlay with landslide inventory map
Multiplication Standardization
Population Vulnerability Map (PVM)
Determination of frequency distributions in landslide locations
Population Freq. LF
0<POP≤0.2 →0.061
0.2<POP≤0.4 →0.523
0.4<POP≤0.6 →0.276
0.6<POP≤0.8 →0.094
0.8<POP≤1.0 →0.046
Spatial impact map for population (SIpop)
Explanations:
SI: Spatial Impact
RL: Relative Loss
LF: Landslide Frequency
AHP: Analythical Hierarchy Process

◀ **Fig. 11** Flow chart representing the calculation of spatial impact and relative loss of elements at risk: **a** environmental, **b** infrastructural and **c** population

groups ranging from very low (1) to very high (5) vulnerability:

$$EV = SI_{env} * RL_{env} \quad (8)$$

$$IV = SI_{inf} * RL_{inf} \quad (9)$$

$$PV = SI_{pop} * RL_{pop} \quad (10)$$

$$RVI = EV + IV + PV \quad (11)$$

where EV is the environmental vulnerability, IV is the infrastructural vulnerability, PV is the population vulnerability, SI is the spatial impact for the elements at risk group (i. e. environmental, infrastructural and population), RL is relative loss for the elements-at-risk group (i.e. environmental, infrastructural and population) and RVI is the relative vulnerability index.

Results and discussion

At the final stage of the study, a semi-quantitative landslide risk index (LRI) map was produced by considering the LHI and RVI maps. LRI was achieved by combining the LHI and RVI maps, expressing the specific risk throughout the study area. For the combination of LHI and RVI, we took into consideration a semi-quantitative risk matrix ranging from very low (1) to very high (5) classes, which is tabulated in Table 6. Considering the LHI and RVI classes tabulated in Table 6, the final LRI map was produced (Fig. 13). This map provides a general overview on the landslide risk phenomenon in the study area. In other words, it could be considered as an initial step with respect to landslide risk assessments in the study area. According to this map, the northern part of the region was abundantly classified in the VL group, while the close surrounding regions to the city centre (except for the southern part of the city centre) were in the high and very high LRI classes. This means that LHI and RVI values were relatively high. Areal coverages of the LRI classes were calculated as 21.4% very low (VL), 10.8% as low (L), 37.4% as medium (M), 24.8% as high (H) and 5.6% as very high (VH) LRI, respectively. These values were 19.1% and 10.6%, 23.3% and 31.3%, 27.6% and 31.6%, 20.2% and 22.2%, and 9.8% and 4.3%, corresponding to the classes of VL, L, M, H and VH components, for hazard (LHI) and vulnerability (RVI), respectively. These differences could be explained by the hazard and vulnerability components of LRI. For example, a region with a very high class of vulnerability may be in a very low hazard class, or vice versa. If these classes were combined together based on the class values given in Table 6, the resulting class would be low LRI.

As a general point of view of landslide characteristics, a total of 215 deep-seated rotational earth slides were mapped during the field studies. It was revealed that the landslides in the study area generally occurred in low to medium slope angles. The landslides in the region were mostly observed in a weathering zone of weak flysch units, formed by siltstone, mudstone and sandstone alternations with occasionally volcanic intercalations. The landslides in the study area generally occurred on the northeastern-facing slopes with topographical elevations between 1000 and 1250 m (asl). The most common land cover types of landslides are orchards (25.72%), mixed agricultural area (20.42%) and olive groves (16.60%). In landslide susceptibility analyses, FR and LR models were taken into consideration. In the performance evaluations, the AUC values were calculated as 0.828 for the LR method and 0.862 for the FR method, respectively. Due to its higher AUC value, the FR model susceptibility map was selected as the main input component for hazard analysis. For the hazard stage, precipitation and peak ground acceleration parameters were

Table 4 AHP matrix used in economic valuation of vulnerability assessments for the components of land use categories

Elements	Urban Area	Plantation	Agricultural Area	Forest	Bare Land	Water
Urban Area	1					
Plantation	1/6	1				
Agricultural Area	1/5	2	1			
Forest	1/4	4	2	1		
Bare Land	1/9	1/5	1/7	1/8	1	
Water	1/5	1/2	1/3	1/5	3	1
Weight	0.459	0.088	0.140	0.226	0.027	0.060

*CR: 0.08 (consistent)

Table 5 AHP matrix used in economic valuation of vulnerability assessments for the components of infrastructural elements

Elements	RAI	NGP	PWL	PWP	WCH	RON
RAI	1					
NGP	3	1				
PWL	1/2	1/5	1			
PWP	1/3	1/6	1/3	1		
WCH	1/4	1/7	1/4	2	1	
RON	2	1/3	3	4	5	1
Weight	0.151	0.421	0.109	0.046	0.052	0.221

CR: 0.07 (consistent)

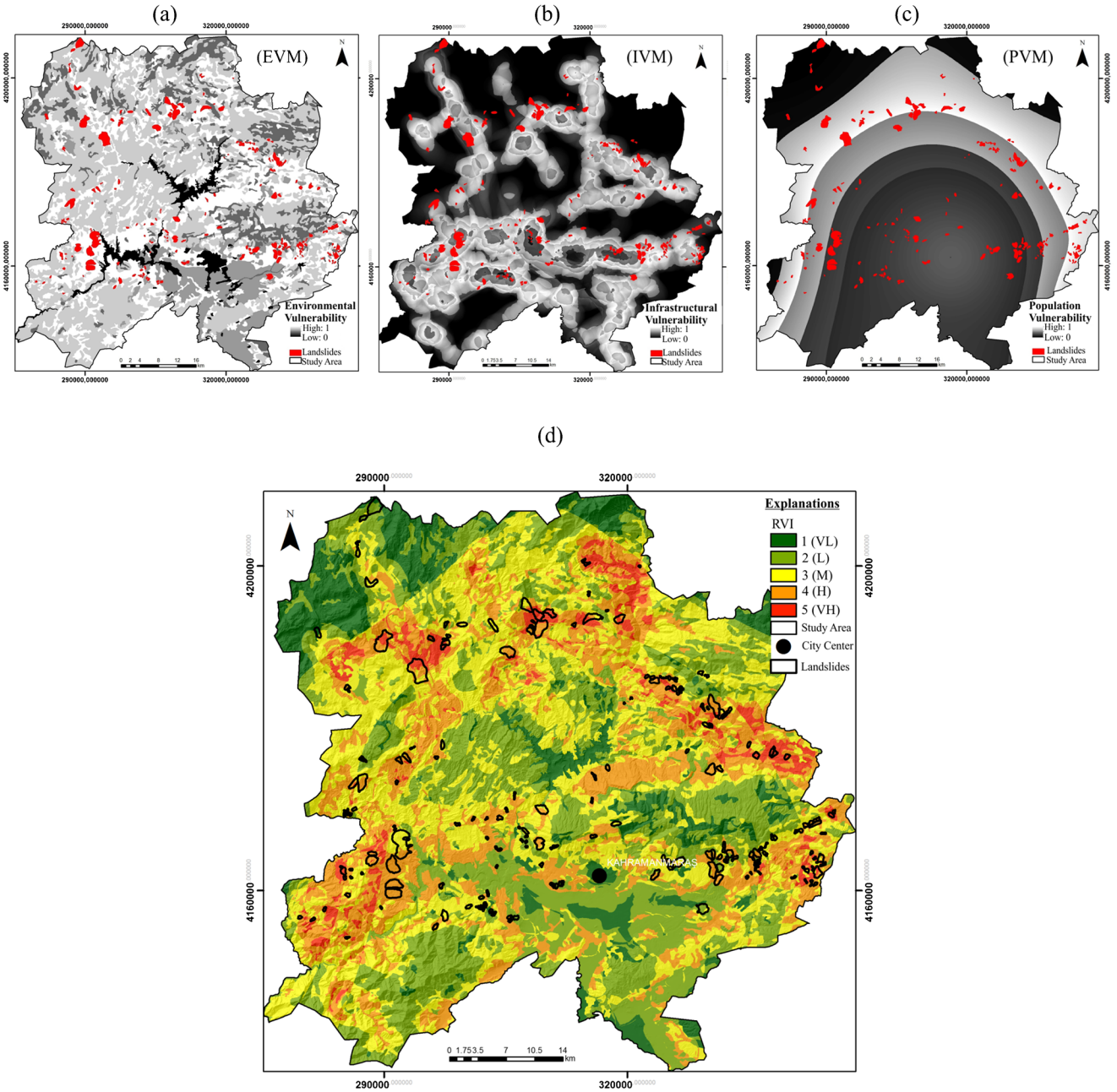

Fig. 12 Vulnerability maps for the study area: **a** environmental vulnerability map (EVM), **b** infrastructural vulnerability map (IVM), **c** population vulnerability map (PVM) and **d** relative vulnerability (RVI) map

Table 6 Semi-quantitative risk matrix used in the study

LHI classes	RVI classes				
	1 (VL)	2 (L)	3 (M)	4 (H)	5 (VH)
1 (VL)	1 (VL)	1 (VL)	1 (VL)	2 (L)	2 (L)
2 (L)	1 (VL)	2 (L)	3 (M)	3 (M)	4 (H)
3 (M)	1 (VL)	3 (M)	3 (M)	4 (H)	4 (H)
4 (H)	2 (L)	3 (M)	4 (H)	4 (H)	5 (VH)
5 (VH)	2 (L)	4 (H)	4 (H)	5 (VH)	5 (VH)

considered. Although there were no data related to the earthquake-triggered landslides in the region, closeness to the active fault zones of the study area was the main reason for this selection (20% effect in triggering indicators in hazard stage). Based on the archive studies and the interviews with local people, most of the landslides was triggered after a long-term heavy rainfall. There was also a good harmony between the higher precipitation values and the number of landslides. Thus, 80% weight was given to the triggering indicator for LHI calculation.

It was almost impossible to assess the temporal vulnerability in such a region and data scarcity. Thus, it was preferred to assess the spatial vulnerability comparing the considered elements at risk, relatively. In other words, it was not intended to assess an individual element at risk in the region such as a building, road cut, etc. The main idea herein was to represent the spatial vulnerability with respect to each group of elements at risk. The economic valuation of vulnerability stage was performed by the AHP model. However, it should not be considered as an insufficient approach since it would provide

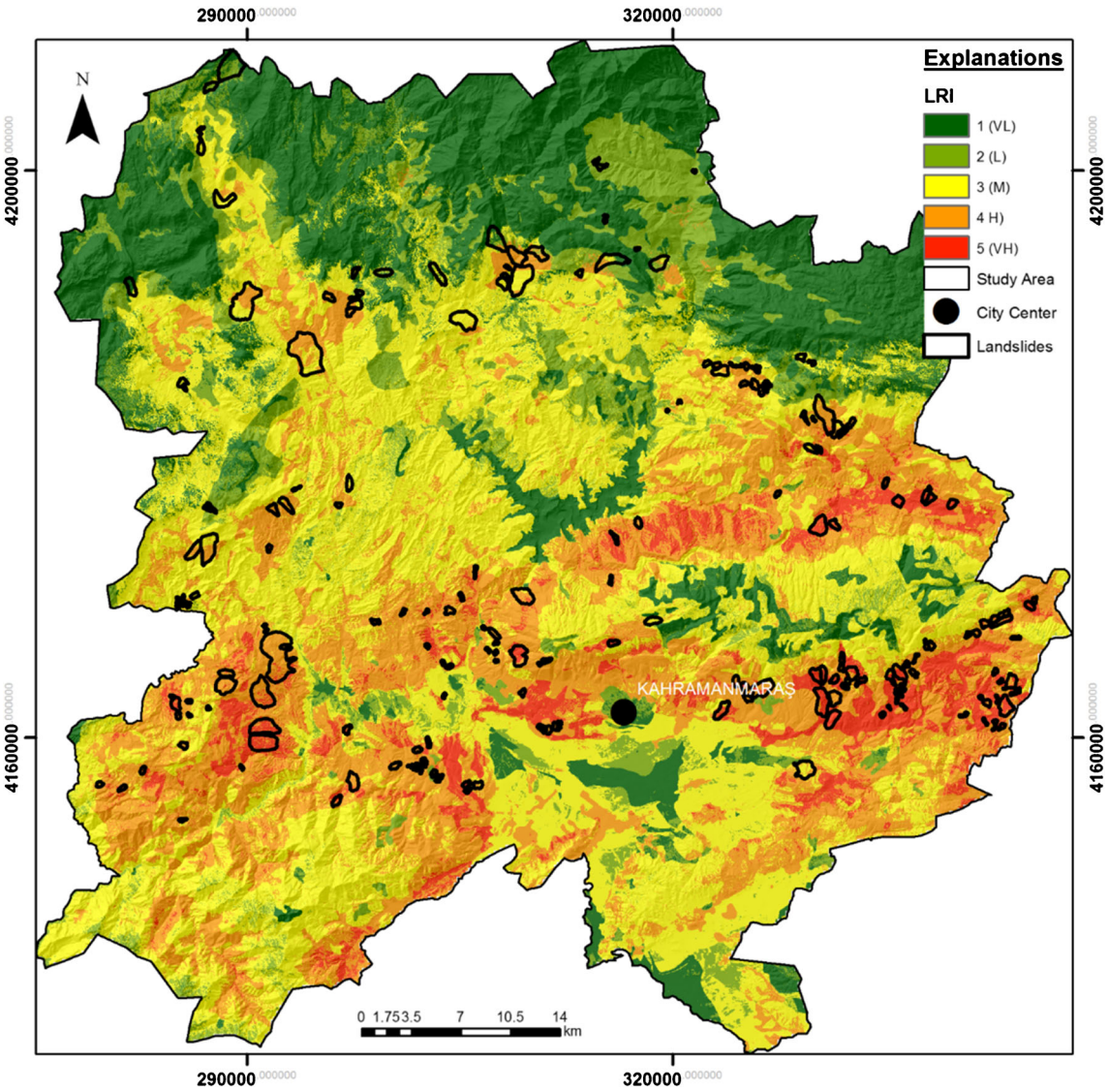

Fig. 13 LRI map of the study area

valuable information based on the experience and judgement of the experts, particularly in data-scarce environments. For the vulnerability assessments, two indicators, namely spatial impact (SI) and relative loss (RL), were introduced. These indicators were associated with the degree of loss and magnitude and/or intensity components of the term vulnerability given by Varnes and IAEG (1984). Degree of loss and magnitude (to some extent, intensity) components of vulnerability were imitated by RL and SI, respectively. For the losses, economic valuation of RL for environmental and infrastructural elements at risk was performed by using the AHP model. Based on the results of the AHP model, urban area class was the most valued one for environmental elements at risk. For infrastructural elements, the most valued element was natural gas pipeline. For population data, population density map was used for this purpose (i.e. relative loss) since it was not logical to compare human life with another type of element at risk by using AHP. As for the spatial impacts of the elements at risk, it was assessed based on the spatial distributions of these elements located on the landslides. Spatial impact values of the elements at risk were calculated by landslide frequencies based on their spatial distributions. For this indicator, it was linked to the intensity or magnitude of a landslide. It was thought that an element at risk was further damaged if the intensity or magnitude of the landslide of concern was higher than that of the other landslides. Thus, spatial distribution on landslide locations (i.e. LF) of any element at risk could be more expected to expose a landslide. For example, in the case of the RAI and NGP components of infrastructural elements, there were no landslide locations with respect to areal extents since the LF values were 0 for their all subgroups. However, NGP and RAI were two of the most valued components (NGP, the first one; RAI, the third one) of infrastructural elements based on the economic valuation (see Table 5). It means that there will be a possible economic loss if a landslide occurs, but since they have no spatial impact, infrastructural vulnerability will be zero for these components. However, environmental and/or population vulnerability may exist in the areas covered by NGP and RAI components. For this reason, environmental, infrastructural and population vulnerabilities were added arithmetically to produce the RVI map.

Conclusions

The practical utilization of the so-produced LRI map in regional planning of the study area is very important in the future. It is thought that the utilization of such maps, which will be very beneficial especially for decision makers and local administrations, will also play an important role in minimizing the damages caused by landslides. In the light of all these assessments, it is clear that landslides and their consequences will pose serious problems for the region in the future, regardless of considering the population growth. Apart from the city centre, there were many scattered settlements located in medium- to very-high-LRI zones in the study area (corresponding approximately to 70% areal coverage for these classes). Since this approach is the initial step of highlighting the landslide risk assessment of the region, detailed analyses should be performed in these zones in addition to the database improvement.

It was important to conduct such a work to highlight the landslide risk conditions based on the available data for the study area. However, it should be kept in mind that it can be re-evaluated with some additional studies when the data deficiencies are eliminated in the future. It is inevitable in data-scarce regions that some certain assumptions should be made. In this context, it is considered that the public institutions and organizations, especially the decision makers, local administrations and universities, have significant responsibilities to produce and to transfer reliable and high-quality data not only for landslides but also for all natural hazards for future works.

Acknowledgements The authors would like to thank to the AFAD Provincial Directorate of Kahramanmaraş team, Department of Planning and Mitigation and Department of Earthquake of AFAD Central Presidency personnel for their kind help during the field studies and providing data related to the study.

References

Abella EAC, Van Westen C (2007) Generation of a landslide risk index map for Cuba using spatial multi-criteria evaluation. Landslides 4: 311–325

Achour Y, Garçia S, Cavaleiro V (2018) GIS-based spatial prediction of debris flows using logistic regression and frequency ratio models for Zêzere River basin and its surrounding area, Northwest Covilhã, Portugal. Arab J Geosci 11:550

Aditian A, Kubota T, Shinohara Y (2018) Comparison of GIS-based landslide susceptibility models using frequency ratio, logistic regression, and artificial neural network in a tertiary region of Ambon, Indonesia. Geomorphol 318:101–111

Akgun A, Kıncal C, Pradhan B (2012) Application of remote sensing data and GIS for landslide risk assessment as an environmental threat to Izmir city (west Turkey). Environ Monit Assess 184:5453–5470

Aleotti P, Chowdhury R (1999) Landslide hazard assessment: summary review and new perspectives. Bull Eng Geol Environ 58(1):21–44

Alkevli T, Ercanoglu M (2011) Assessment of ASTER satellite images in landslide inventory mapping: Yenice-Gökçebey (Western Black Sea Region, Turkey). Bull Eng Geol Environ 70:607–617

Arca D, Citiroglu HK, Tasoglu İK (2019) A comparison of GIS-based landslide susceptibility assessment of the Satuk village (Yenice, NW Turkey) by frequency ratio and multicriteria decision methods. Environ Earth Sci 78:81

Bai S, Lu P, Wang J (2015) Landslide susceptibility assessment of the Youfang catchment using logistic regression. J Mt Sci 12(4):816–827

Bednarik M, Yılmaz I, Marschalko M (2012) Landslide hazard and risk assessment: a case study from the Hlohovec–Sered' landslide area in south-west Slovakia. Nat Hazards 64:547–575

Behera R, Kar A, Das MR, Panda PP (2019) GIS-based vulnerability mapping of the coastal stretch from Puri to Konark in Odisha using analytical hierarchy process. Nat Hazards 96:731–751

Bianchini S, Solari L, Casagli N (2017) A GIS-based procedure for landslide intensity evaluation and specific risk analysis supported by persistent scatterers interferometry (PSI). Remote Sens 9(1093):1–20

Catani F, Casagli N, Ermini L, Righini G, Menduni G (2005) Landslide hazard and risk mapping at catchment scale in the Arno River basin. Landslides 2:329–342

Chen T, Niu R, Jia X (2016) A comparison of information value and logistic regression models in landslide susceptibility mapping by using GIS. Environ Earth Sci 75:867

Chen W, Pourghasemi HR, Panahi M, Kornejady A, Wang J, Xie X, Cao S (2017) Spatial prediction of landslide susceptibility using an adaptive neuro-fuzzy inference system combined with frequency ratio, generalized additive model, and support vector machine techniques. Geomorphol 297:69–85

Chen W, Hong H, Panahi M, Shahabi H, Wang Y, Shirzadi A, Pirasteh S, Alesheikh AA, Khosravi K, Panahi S, Rezaie F, Li S, Jaafari A, Bui DT, Ahmad BB (2019a) Spatial prediction of landslide susceptibility using GIS-based data mining techniques of ANFIS with Whale Optimization Algorithm (WOA) and Grey Wolf Optimizer (GWO). Appl Sci 9:3755

Chen W, Yan X, Zhao Z, Hong H, Bui DT, Pradhan B (2019b) Spatial prediction of landslide susceptibility using data mining-based kernel logistic regression, naive Bayes and RBF network models for the Long County area (China). Bull Eng Geol Environ 78:247–266

Corominas J, Van Westen C, Frattini P, Cascini L, Malet JP, Fotopoulou S, Catani F, Van Den Eeckhaut M, Mavrouli O, Agliardi F, Pitilakis K, Winter MG, Pastor M, Ferlisi S, Tofani V, Herva's J, Smith JT (2014) Recommendations for the quantitative analysis of landslide risk. Bull Eng Geol Environ 73(2):209–263

Dai FC, Lee CF, Ngai YY (2002) Landslide risk assessment and management: an overview. Eng Geol 64:65–87

Di Martire D, Paci M, Confuorto P, Costabile S, Guastaferro F, Verta A, Calcaterra D (2017) A nation-wide system for landslide mapping and risk management in Italy: the second not-ordinary plan of environmental remote sensing. Int J Appl Earth Obs Geoinf 63:147–157

Du G, Zhang Y, Iqbal J, Yang Z, Yao X (2017) Landslide susceptibility mapping using an integrated model of information value method and logistic regression in the Bailongjiang watershed, Gansu Province, China. J Mt Sci 4(2):249–268

Eastman R (2012) The IDRISI Selva help. Clark University, Worcester MA

Evans SG, Roberts NJ (2006) A country-specific geo-risk index (GRI); a first approximation to partitioning the contribution of hazard and vulnerability. Geophys Res Abstr 8:10089

Fell R, Corominas J, Bonnard C, Cascini L, Leroi E, Savage WZ (2008a) Guidelines for landslide susceptibility, hazard and risk zoning for land-use planning. Eng Geol 102(3–4):85–98

Fell R, Corominas J, Bonnard C, Cascini L, Leroi E, Savage WZ (2008b) Guidelines for landslide susceptibility, hazard and risk zoning for land-use planning. Eng Geol 102(3–4):99–111

Galli M, Guzzetti F (2007) Landslide vulnerability criteria: a case study from Umbria, Central Italy. Environ Manag 40:649–664

Gholami M, Ghachkanlu EN, Khosravi K, Pirasteh S (2019) Landslide prediction capability by comparison of frequency ratio, fuzzy gamma and landslide index method. J Earth Sci 128:42

Giannakidou C, Diakoulaki D, Memos CD (2019) Implementing a flood vulnerability index in urban coastal areas with industrial activity. Nat Hazards 97:99–120

Gonçalves CG, Zezere JL (2018) Combining social vulnerability and physical vulnerability to analyse landslide risk at the municipal scale. Geosci 8(8):294: 1–17

Guzzetti F, Carrara A, Cardinali M, Reichenbach P (1999) Landslide hazard evaluation: a review of current techniques and their application in a multi–scale study, Central Italy. Geomorphol 31:181–216

Guzzetti F, Cardinali M, Reichenbach P, Carrara A (2000) Comparing landslide maps: a case study in the upper Tiber River basin, Central Italy. Environ Manag 25(3):247–363

Jaedicke C, Nadim F, Kalsnes B, Vangelsten B, Sverdrup-Thygeson K, Syre E, Smebye H, Van Den Eeckhaut M, Hervás J, Smith J, Winter M, Tofani V, Ciurean R (2014) Identification of landslide hazard and risk 'hotspots' in Europe. Bull Eng Geol Environ 73(2):325–339

Jana SK, Sekac T, Pal DK (2019) Geo-spatial approach with frequency ratio method in landslide susceptibility mapping in the Busu River catchment, Papua New Guinea. Spat Inf Res 27(1):49–62

Kadavi PR, Lee CV, Lee S (2019) Landslide-susceptibility mapping in Gangwon-do, South Korea, using logistic regression and decision tree models. Environ Earth Sci 78:116

Köhle MP, Neuhauser B, Ratzinger K, Wenzel H, Howes DD (2007) Elements at risk as a framework for assessing the vulnerability of communities to landslides. Nat Hazards Earth Syst Sci 7:765–779

Lee S, Sambath T (2006) Landslide susceptibility mapping in the Damrei Romel area, Cambodia using frequency ratio and logistic regression models. Environ Geol 50:847–855

Leone F, Aste JP, Leroi E (1996) Vulnerability assessment of elements exposed to mass-moving: working toward a better risk perception. In: Senneset K (ed) Landslides. Balkema, Rotterdam, pp 263–269

Li L, Liu R, Pirasteh S, Chen X, He L, Li J (2017) A novel genetic algorithm for optimization of conditioning factors in shallow translational landslides and susceptibility mapping. Arab J Geosci 10:209

Lombardo L, Cama M, Conoscenti C, Marker M, Rotigliano E (2015) Binary logistic regression versus stochastic gradient boosted decision trees in assessing landslide susceptibility for multiple-occurring landslide events: application to the 2009 storm event in Messina (Sicily, southern Italy). Nat Hazards 79:1621–1648

Mandal S, Mandal K (2018) Modeling and mapping landslide susceptibility zones using GIS based multivariate binary logistic regression (LR) model in the Rorachu river basin of eastern Sikkim Himalaya, India. Model Earth Syst Environ 4:69–88

Mandal SP, Chakrabarty A, Maity P (2018) Comparative evaluation of information value and frequency ratio in landslide susceptibility analysis along national highways of Sikkim Himalaya. Spat Inf Res 26(2):127–141

Meten M, Bhandary NP, Yatabe R (2015) GIS-based frequency ratio and logistic regression modelling for landslide susceptibility mapping of Debre Sina Area in Central Ethiopia. J Mt Sci 12(6):1355–1372

MGM (2019) Ministry of Agriculture and Forestry, General Directorate of Meteorology. http://www.mgm.gov.tr (Accessed May 2019)

Miranda FN, Ferreira TM (2019) A simplified approach for food vulnerability assessment of historic sites. Nat Hazards 96:713–730

Mondal S, Maiti R (2013) Integrating the analytical hierarchy process (AHP) and the frequency ratio (FR) model in landslide susceptibility mapping of Shiv-Khola watershed, Darjeeling Himalaya. Int J Disaster Risk Sci 4(4):200–212

Nadim F, Kjekstad O, Peduzzi P, Herold C, Jaedicke C (2006) Global landslide and avalanche hotspots. Landslides 3(2):159–174

Nandi A, Shakoor A (2009) A GIS-based landslide susceptibility evaluation using bivariate and multivariate statistical analyses. Eng Geol 110:11–20

Nicu IC (2017) Frequency ratio and GIS-based evaluation of landslide susceptibility applied to cultural heritage assessment. J Cult Herit 28:172–176

Nsengiyumva JB, Luo G, Amanambu AC, Mind'je R, Habiyaremye G, Karamage F, Ochege FU, Mupenzi C (2019) Comparing probabilistic and statistical methods in landslide susceptibility modeling in Rwanda/Centre-Eastern Africa. Sci Total Environ 659:1457–1472

Pham BT, Bui DT, Prakash I, Nguyen LH, Dholakia MB (2017a) A comparative study of sequential minimal optimization-based support vector machines, vote feature intervals, and logistic regression in landslide susceptibility assessment using GIS. Environ Earth Sci 76:371

Pham BT, Bui DT, Prakash I (2017b) Landslide susceptibility assessment using bagging ensemble based alternating decision trees, logistic regression and J48 decision trees methods: a comparative study. Geotech Geol Eng 35:2597–2611

Pirasteh S, Li J (2017a) Landslides investigations from geoinformatics perspective: quality, challenges, and recommendations. Geomat Nat Hazard Risk 8(2):448–465

Pirasteh S, Li J (2017b) Probabilistic frequency ratio (PFR) model for quality improvement of landslide susceptibility mapping from LiDAR-derived DEMs. Geoenv Disaster 4:19

Pirasteh S, Shamsipour G, Liu G, Zhu Q, Chengming YE (2020) A new algorithm for landslide geometric and deformation analysis supported by digital elevation models. Earth Sci Inf 13:361–375

Polykretis C, Chalkias C (2018) Comparison and evaluation of landslide susceptibility maps obtained from weight of evidence, logistic regression, and artificial neural network models. Nat Hazards 93:249–274

Raja NB, Çiçek I, Türkoğlu N, Aydın O, Kawasaki A (2017) Landslide susceptibility mapping of the Sera River Basin using logistic regression model. Nat Hazards 85:1323–1346

Regmi AD, Yoshida K, Pourghasemi HR, Dhital MR, Pradhan B (2014) Landslide susceptibility mapping along Bhalubang–Shiwapur area of mid-Western Nepal using frequency ratio and conditional probability models. J Mt Sci 11(5):1266–1285

Rehman S, Sahana M, Hong H, Sajjad H, Ahmed BB (2019) A systematic review on approaches and methods used for food vulnerability assessment: framework for future research. Nat Hazards 96:975–998

Saaty TL (1977) A scaling method for priorities in hierarchical structures. J Math Psychol 15:234–281

Saaty TL (2008) Decision making with the analytic hierarchy process. Int J Serv Sci 1(1):83–98

Sahana M, Sajjad H (2017) Evaluating effectiveness of frequency ratio, fuzzy logic and logistic regression models in assessing landslide susceptibility: a case from Rudraprayag district, India. J Mt Sci 14(11):2150–2167

Sangchini EK, Emami SN, Tahmasebipour N, Pourghasemi HR, Naghibi SA, Arami SA, Pradhan B (2016) Assessment and comparison of combined bivariate and AHP models with logistic regression for landslide susceptibility mapping in the Chaharmahal-e-Bakhtiari Province, Iran. Arab J Geosci 9:201

Sassa K (2017) The 2017 Ljubljana Declaration on landslide risk reduction and the Kyoto 2020 Commitment for global promotion of understanding and reducing landslide disaster risk. Landslides 14: 1289–1296

Singh A, Kanungo DP, Pal S (2019a) Physical vulnerability assessment of buildings exposed to landslides in India. Nat Hazards 96:753–790

Singh A, Kanungo DP, Pal S (2019b) A modified approach for semi-quantitative estimation of physical vulnerability of buildings exposed to different landslide intensity scenarios. Georisk 13(1):66–81

Solaimani K, Mousavi SZ, Kavian A (2013) Landslide susceptibility mapping based on frequency ratio and logistic regression models. Arab J Geosci 6:2557–2569

Soma AS, Kubota T, Mizuno H (2019) Optimization of causative factors using logistic regression and artificial neural network models for landslide susceptibility assessment in Ujung Loe watershed, South Sulawesi Indonesia. J Mt Sci 16(2):383–401

Sümengen M (2013) 1/100000 scale Turkey geological map series, H37 quadrangle. No: 188. General Directorate of Mineral Research and Exploration, Ankara, (in Turkish)

Talaei R (2014) Landslide susceptibility zonation mapping using logistic regression and its validation in Hashtchin Region, northwest of Iran. J Geol Soc India 84:68–86

Totsching R, Fuchs S (2013) Mountain torrents: quantifying vulnerability and assessing uncertainties. Eng Geol 155:31–44

Van Den Eeckhaut M, Herva's J (2012) State of the art of national landslide databases in Europe and their potential for assessing landslide susceptibility, hazard and risk. Geomorphol 139–140:545–558

Van Westen CJ, Van Asch TWJ, Soeters R (2006) Landslide hazard and risk zonation-why is it still so difficult? Bull Eng Geol Environ 65(2):167–184

Varnes DJ, IAEG Commission on Landslide (1984) Landslide hazard zonation: a review of principles and practice. UNESCO, Paris

Wang L, Guo M, Sawada K, Lin J, Zhang J (2016) A comparative study of landslide susceptibility maps using logistic regression, frequency ratio, decision tree, weights of evidence and artificial neural network. Geosci J 20–1:117–136

Wu Y, Li W, Wang Q, Liu Q, Yang D, Xing M, Pei Y, Yan S (2016) Landslide susceptibility assessment using frequency ratio, statistical index and certainty factor models for the Gangu County, China. Arab J Geosci 9:84

Wu Z, Wu Y, Yang Y, Chen F, Zhang N, Ke Y, Li W (2017) A comparative study on the landslide susceptibility mapping using logistic regression and statistical index models. Arab J Geosci 10:187

Yan F, Zhang Q, Ye S, Ren B (2019) A novel hybrid approach for landslide susceptibility mapping integrating analytical hierarchy process and normalized frequency ratio methods with the cloud model. Geomorphol 327:170–187

Ye C, Li Y, Li L, Pirasteh S, Cui P, Li J (2019) Landslide detection of hyperspectral remote sensing data based on deep learning with constrains. IEEE J Sel Top Appl Earth Obs Remote Sens 12(12):5047–5060

Yoshimatsu H, Abe S (2006) A review of landslide hazards in Japan and assessment of their susceptibility using an analytical hierarchic process (AHP) method. Landslides 3:149–158

Youssef AM, Al-Katheeri M, Pradhan B (2015) Landslide susceptibility mapping at Al-Hasher Area, Jizan (Saudi Arabia) using GIS-based frequency ratio at index of entropy models. Geosci J 19(1):123–134

Zhang M, Cao X, Peng L, Niu R (2016a) Landslide susceptibility mapping based on global and local logistic regression models in Three Gorges Reservoir area, China. Environ Earth Sci 75:958

Zhang Z, Yang F, Chen H, Wu Y, Li T, Li W, Wang Q, Liu P (2016b) GIS-based landslide susceptibility analysis using frequency ratio and evidential belief function models. Environ Earth Sci 75:948

Zhu A, Miao Y, Yang L, Bai S, Liu J, Hong H (2018) Comparison of the presence-only method and presence-absence method in landslide susceptibility mapping. Catena 171:222–233